universität wien

DIPLOMARBEIT / DIPLOMA THESIS

Titel der Diplomarbeit / Title of the Diploma Thesis

„Combined diffused light imaging and computed tomography to evaluate an orthotopic canine breast cancer xenograft model“

verfasst von / submitted by

Simone Mezgolits

angestrebter akademischer Grad / in partial fulfilment of the requirements for the degree of

Magistra der Pharmazie (Mag.pharm.)

Wien, 2017 / Vienna, 2017

Studienkennzahl lt. Studienblatt / degree programme code as it appears on the student record sheet:	A 449
Studienrichtung lt. Studienblatt / degree programme as it appears on the student record sheet:	Diplomstudium Pharmazie
Betreut von / Supervisor:	Univ.-Prof. Dipl.-Ing. Dr. Manfred Ogris

Acknowledgements

At this point I would like to say “thank you” to all the people who supported me during my studies. First of all I would like to thank my parents Irina and Martin, who believed in me and my abilities from the very first second of my life. Then also big thanks to my family and friends for their support and their just being there when I needed them. Speaking of my friends, I would like to thank especially Dr. Sebastian Gehrig for supervising me and sharing his knowledge, expertise and coffee with me. He was always a helping hand and I am glad that we became friends during my time at the MMCT lab. And finally a big “thank you” to Prof. Ogris and the members of his research team for giving me the opportunity to do my diploma thesis at the MMCT lab.

Table of contents

Table of contents 1

Abstract 2

Zusammenfassung 3

1. Introduction 4

1.1. Micro Computed Tomography (µCT) 6

1.1.1. Basic Principle 6

1.1.2. Construction of a µCT scanner 6

1.1.3. Contrast agents for µCT 6

1.1.4. Advantages and limitations of µCT 7

1.2. Bioluminescence Imaging (BLI) 7

1.3. Three dimensional Diffuse Light Imaging Tomography (DLIT) 9

1.4. Multimodal Imaging BLI/µCT and DLIT/µCT 9

1.5. Tumour micro-environment and combined µCT/DLIT 10

2. Aim of the project 10

3. Materials and methods 11

3.1. Cell line and cell transduction 11

3.2. Cell Culture 11

3.3. Animals 11

3.4. In vivo tumour model 11

3.5. Imaging procedures 12

3.6. Living Image ™ Software for image analysis and tomographic reconstruction 13

3.7. Amira® Software for tumour segmentation and volume measurement 14

3.8. Histology 15

3.9. HE-staining 15

3.10. Microscopy 16

4. Results 17

Animal 91 24

Animal 92 27

Animal 93 30

Animal 94 35

Animal 95 41

5. Discussion 45

6. References 47

Abstract

Breast cancer is one of the most common malignant diseases among humans, but also in pet dogs and show similarities in both species. Thus the development of canine xenograft tumour models in mice is of high importance, considering dogs as patients, but also as large animal models for further preclinical development of anticancer drugs. Combined optical and micro computed tomography (µCT) allows studying tumour growth and dissemination of tumour cells labelled with luciferase (luc) as reporter gene. The focus of the diploma thesis was the evaluation of an imageable spontaneously metastasizing model of canine breast cancer xenografted in mice for future research concerning cancer therapeutics for both human and dog patients, in terms of a clinical comparative oncology. CMT-U27 canine breast cancer cells genetically labelled with the reporter gene firefly luciferase were implanted orthotopically into the mammary fat pad of six female nude mice. The animals were imaged regularly using the IVIS™ Spectrum CT imaging system, to monitor the development and distribution of the tumour cells. DLIT (diffused light imaging) reconstruction was performed using Living Image™ software and tumour signal strength and signal location were measured. Based on the obtained µCTs the tumour volume was measured using Amira™ software. Primary tumours were excised due to their signal strength for a better detection of smaller signals. Finally the animals were dissected and the tumours were further histologically processed. The tumour development and spread could be successfully visualized and measured in the nude mice using these imaging techniques. The results also showed specific distribution patterns of the light signal within the primary tumours. Combined DLIT and µCT turns out to be a suitable method for tracking luc transfected CMT-U27 cells in nude mice.

Zusammenfassung

Brustkrebs ist eine der häufigsten malignen Erkrankungen, sowohl beim Menschen, als auch beim Hund und zeigt sehr große Ähnlichkeiten zwischen den beiden Spezies. Deshalb ist die Entwicklung von xenograft Hundebrustkrebsmodellen in Mäusen von großer Bedeutung, einerseits für den Hund als Patienten und andererseits auch als großes Tiermodell für die weitere präklinische Entwicklung von Antitumor-Arzneistoffen. Kombiniertes optisches und Mikro-Computertomographie-Imaging macht das Erforschen von Tumorwachstum und der Dissemination von Tumorzellen, die mit Luciferase als Reportergenen markiert wurden, möglich. Der Fokus der Diplomarbeit lag auf der Evaluierung eines spontan metastasierenden Hundebrustkrebsmodells in Nacktmäusen, analysiert mit DLIT/µCT, im Hinblick auf spätere Forschung im Bereich der Tumortherapie für Menschen und Hunde, im Sinne einer klinischen komparativen Onkologie. Hundebrustkrebszellen der Zelllinie CMT-U27, genetisch markiert mit dem Reportergen Firefly-Luciferase, wurden orthotop in das Brustgewebe von sechs weiblichen Nacktmäusen implantiert. Die Tiere wurden regelmäßig mittels IVIS™ Spectrum CT auf Entwicklung und Verteilung der Tumorzellen überprüft. Die DLIT-Rekonstruktion wurde mittels Living Image™ Software gemacht und die Tumorsignalstärke und ihre Position wurden ermittelt. Das Tumorvolumen wurde auf Basis des erhaltenen CTs außerdem mittels Amira™ Software ermittelt. Die mit der Zeit entstandenen Primärtumoren wurden operativ entfernt, damit kleinere Biolumineszenzsignale nicht durch das große Signal des Primärtumors überdeckt werden. Schließlich wurden die Tiere seziert und die Tumoren wurden weiter histologisch aufgearbeitet. Das Tumorwachstum und ihre Dissemination konnten erfolgreich mit den angewendeten Methoden visualisiert werden. Die Resultate zeigten auch spezifische Verteilungsmuster innerhalb der Tumoren. Kombinierte DLIT/µCT hat sich als gute Methode für das Nachverfolgen von luc transfizierten CMT-U27 Zellen in Nacktmäusen herausgestellt.

1. Introduction

Breast cancer is the most common malignant disease in western women and the most common neoplasm in female dogs [1,2]. It develops from the mammary gland and has the ability to infiltrate tissue and metastasize to different parts of the body.

The clinical survival rate of metastasized cancer remains poor, although there are a lot of highly effective pre-clinical anti-cancer therapeutics available. A lot of genetic, environmental, immunological, toxic and random factors work together in cancerogenesis [3] and therapy is limited because of the complexity of cancer regarding its anatomy, physiology [4, 5] and heterogeneity [6]. There is no reproducibility of the complex interplay of these factors contributing to disease development and therapy resistance, despite the currently gladly used genetically engineered rodent models, which at the moment only mirror certain aspects of cancer biology. Therefore, a refinement of the models and analysis methods is needed in combination with the introduction of new paradigms in the drug development path. Promising approaches are employment of rodent models generated by orthotopic implantation of tumour cells, mirroring human cancer biology more closely in terms of tumour micro-environment and occurrence of spontaneous metastases [7].

Furthermore the inclusion of pet dog cancer patients in the drug development path promises reliable translation into human oncology, as both species are similar concerning cancer biology, exposure to risk factors and response to conventional therapy [8]. Dog cancers parallel the natural progression of human cancers more closely, than it is observed in induced cancer animal models. This concept, called clinical comparative oncology, also focuses on the fact that the restricted genomic variations of specific dog breeds create a high risk model for breed specific diseases due to consanguinity and inbreeding [9].

For example : The metastatic sites of breast cancer in humans and dogs are quite similar, like lung, liver and bone [1, 2] (Table.I).

The classical, invasive way of examining laboratory animals is to induce the disease in a representative amount of animals and then kill them at different timepoints, in order to analyze the progression of the disease.

Contrary molecular imaging allows the non-invasive and real time visualization of biological processes in vivo. This method collects longitudinal data and therefore reduces the number of experimental animals and costs [10]. Animals act as their own controls and inter individual differences do not play a role anymore [11]. From an ethical point of view, imaging is one of

the best techniques to decrease the amount of laboratory animals needed in cancer research, and is therefore of great value to life sciences and medicine.

	HUMAN	**DOG**
Lung	X	X
Pleura	X	
Liver	X	X
Bone	X	X
Peritoneum	X	
Pancreas	X	X
Spleen	X	X
Skin	X	X
Gastr.int.	X	
Brain	X	X
Heart	X	X
Pericardium	X	
Adr. glands	X	X
Thyroid	X	
Kidney	X	X
Ovary	X	
Uterus	X	X
LN		X
Eye		X
Muscle		X

Table.1: Metastatic sites of human and canine breast cancer
The figures show the similarities between the metastatic behaviour of human and canine breast cancer, e.g. the spread to the lung, liver and bone. [1, 2]

Another advantage of molecular imaging is the ability to detect even a very low number of cells, long before apparent morphological changes in tissue can be seen. In cases of bioluminescence imaging, a functional imaging technique and subgroup of molecular imaging, less than 10 cells can be detected in vivo under optimal conditions [12]. A shortcoming with molecular imaging however, is the lack of morphological information. To overcome this issue, morphological information has to be generated using specific imaging methods, such as micro computed tomography. The combination of functional and morphological imaging results in a multi modal method, which allows the investigation of natural tumour behavior and also provides anatomical references. The distribution of cancerous tissue and its association to organs can be seen, as well as, in cases of therapy, the tissue specific response, which can manifest itself in a reduction in tumour volume and/or a decrease of the bioluminescence signal. Thus, here we investigate the metastatic behavior of CMT-U27 by combined molecular and mor-

phological imaging namely diffuse light imaging tomography (DLIT) and micro computed tomography (µCT).

1.1. Micro Computed Tomography (µCT)

1.1.1. Basic Principle

X-Rays are electromagnetic waves of short wavelength ranging from 10^{-8} to 10^{-11} m. They have the ability to penetrate matter and interact with its electrons. This leads to the attenuation of beam intensity, which always depends on the composition of the object. X-Rays are able to trans-illuminate tissue and provide tissue-specific differences between the attenuation coefficients, which is why we use them.

µCT is a high-resolution derivate of original X-Ray computed tomography [13]. It was first described in the early 1980s [14, 15] and numerous reviews concerning µCT have been published [16, 17].

This medical imaging technique aims at obtaining three-dimensional anatomical information by reconstructing the distribution of the attenuation coefficients of X-Rays which trans-illuminate tissues. The object has to be measured multiple times from various angles to produce cross-sectional images of specific areas, which can then be reconstructed with a computer. [18].

1.1.2. Construction of a µCT scanner

µCT scanners can be constructed in two different ways. The first principle involves a gantry which can rotate around the object that has to be examined. A scanner with an X-Ray detector and a radiation source is fitted to this gantry. The distance between source and detector is set. This construction is also named ,,mini-CT'' because it is like a mini version of the clinical CT used for humans. The second principle involves the rotation of the object within the light path, which allows free adjustment of the distances between source, object and detector [19].

µCT itself shows good results in imaging objects with high atomic numbers, such as bones, but show limitations in contrasting soft tissue. Therefore the use of contrast agents is needed to highlight the required areas.

1.1.3. Contrast agents for µCT

To further enhance the contrast between soft tissue in µCT, exogenous contrast agents are used.

The most commonly used vascular hyperattenuating contrast agents are water soluble and iodine based [20]. Contrast enhancement depends on blood volume, permeability and plasma half-life. Besides iodine based contrast agents, barium is also important. Barium sulfate is commonly used for gastrointestinal investigations as it is insoluble. Iodine-based contrast agents may be incorporated into any organic molecule and can occur in different formulations, e.g. as iodinated lipids, as water-soluble contrast agents or as nanoparticles [21]. The basic structure of many iodine-based contrast-enhancer is the 2,4,6-triiodo-bencoic acid.
Besides the iodine- and barium based contrast agents, there are also other vascular contrast agents available, such as Exitron Nano® (Miltenyi Biotec). This is an earthmetal-based nanoparticular intravascular contrast agent, with a size above the renal excretion limit and a plasma half-life of over 4h. Exitron Nano® is cleared within the retico-endothelial system in the liver and shows hyperattenuation of liver, spleen, lymphnodes and suprarenal glands, up to several weeks post injection [22].

1.1.4. Advantages and limitations of µCT

The advantages of µCT, in comparison to other imaging techniques, are rapid data acquisition, the provision of high resolution images and its good sensitivity to soft and skeletal tissue, especially when using a contrast enhancer [23]. On the other hand, X-Ray also shows some limitations, like the potential safety issue concerning the X-Ray itself. Further, X-Ray suffers from a high intrinsic background signal and is therefore of little value for the imaging of target-specific interaction. But nevertheless microCT is likely to be used for providing an anatomical reference in combination with other molecular imaging modalities.

1.2. Bioluminescence Imaging (BLI)

Bioluminescence is the luminescence (emission of light) from living organisms [24]. It is a reaction between the enzyme luciferase and the substrate luciferin, which occur in certain bacteria, marine crustaceans, fish and insects. Fireflies (*Lucidota*) were the first organisms used for investigating and demonstrating the luciferin-luciferase reaction [25]. After this discovery, continuous research on this topic has led to a better understanding of the firefly bioluminescence, for example the need for ATP as a cofactor [26] and Mg^{2+} as an additive for the reaction [27], the crystallization of luciferase [28] and the chemical synthesis of luciferin [29, 30]. The active form of luciferin is the D-form, while the L-form is the competitive inhibitor of firefly-luciferase [31].

Reaction-scheme of firefly bioluminescence [32]:

(1) $E + LH_2 + ATP + Mg^{2+} \Rightarrow E{\cdot}LH_2\text{-}AMP + PP + Mg^{2+}$

(2) $E{\cdot}LH_2\text{-}AMP + O_2 \Rightarrow E{\cdot}L + CO_2 + AMP + Light$

E… luciferase
LH_2… D-luciferin
PP… pyrophosphate
AMP… adenosine mono phosphate
LH_2-AMP… D-luciferyl adenylate
L… oxyluciferin

The luciferase (luc) gene from the North American firefly *Photinus pyralis* is used as a reporter gene for BLI. In its native form, the enzyme produces light with a maximum wavelength of 560 nm, but can also shift the maximum excitation wavelength above 600 nm with amino acid substitution [33]. Therefore it is possible to use luc for in vivo detection. D-luciferin, the substrate for luc and also many other luciferases, is able to disperse in the whole body, can cross the cell membranes and is non-toxic [34]. As shown in the reaction scheme above, luc requires, beside D-luciferin, also ATP, Mg^{2+} and O_2. Especially the need for oxygen for the light-emitting reaction shows the limitation of BLI. Under hypoxic conditions, e.g. during ischemia or necrosis, enzyme activity and hence light emission will be decreased, which will result in a wrong reflection of luc-expression. Thus, a certain point BLI signal does not entirely reflect tumour load due to changes in the tumour micro environment. Vessels, hypoxic areas, necrosis, connective tissue, immune cells do not contribute to BLI signal.

The luciferase of the sea pansy *Renilla reniformis* (ruc) is another enzyme used for BLI. Its substrate is not luciferin, like for firefly luciferase, but coelenterazine [35].

The difference to firefly luciferase is that renilla luciferase emits blue light at a wavelength of about 480 nm. This is, in comparison to firefly luciferase, a disadvantage for in vivo application. In this spectral range tissue absorption and auto-fluorescence are evident. A big advantage of renilla luciferase, on the other hand, is an ATP-independent ability to emit light, which is a good solution for imaging tissue with a reduced energy status [36]. Research on renilla luciferase has shown that the wavelength of the emitted light can be shifted to longer wavelengths (up to 550 nm) by the mutation of amino acids within the binding site of the enzyme [37].

In order to follow the biodistribution of tumours in vivo, bioluminescence imaging requires the transfection of the cells of choice with a luciferase gene and a promoter. These engineered cells are then injected into the experimental animal. Prior to the imaging process, the substrate has to be administered in order to obtain the light emitting reaction of the transfected cells.

Common ways of their administration are intraperitoneal or intravascular injections. Their dissemination can then be tracked by an imaging system by detecting the location and signal strength [38].

1.3. Three dimensional Diffuse Light Imaging Tomography (DLIT)

Two dimensional tracking of genetically modified cells is a well established tool to follow the biodistribution. Light from bioluminescent sources is emitted in the depth of the animal and detected at its surface. 2D images are generated quickly, but allow only semiquantitative analysis and a rough estimate of signal origin, due to tissue absorption and scattering. Further in-depth localization and therefore exact morphological association of signal and anatomical structure cannot be accomplished in 2D measurement. To overcome these limitations, three dimensional analysis is required. Diffuse light imaging tomography (DLIT) utilizes differences in absorption, depending on the wavelength for a three-dimensional detection of the BLI signal [41]. The first step of this technology consists of reconstructing a virtual surface got by structured light illumination. The second step is the measurement of emitted light at different wavelengths taking the surface topology into account. Here it has to be considered, that tissue absorption of light decreases with the emitted wavelength. After this a calculation of the signal depth by a DLIT algorithm is done. A computed tomographic (CT) maximum intensity projection (MIP) provides the surface topology [42]. With the combination of µCT and DLIT the correct anatomical localization of the tumours can be shown with and also a quantitative analysis of the signal can be done.

With combined µCT and DLIT the tumour load can easily be calculated and as a conclusion from this, the response to therapy of cancerous tissue associated with specific organs and tissues becomes measurable.

1.4. Multimodal Imaging BLI/µCT and DLIT/µCT

BLI and DLIT show good results in investigating tumour progression and detecting tumour metastases in live animal models [39, 40]. In combination with a µCT, which provides the anatomical structure of the animal, a suitable multimodal imaging technique for tumour metastases can be used for cancer research.

1.5. Tumour micro-environment and combined µCT/DLIT

Solid tumours do not only consist of viable oxygenated tumour cells, but also of extracellular matrix, stromal cells, immune cells and leaky vascular structures. All these components form the tumour to an individual kind of organ [43]. Several changes in the tumour micro environment happen during tumour growth. Hypoxia is a central characteristic of solid tumours, which underlies a rapid and uncontrolled growth of tumour cells [44]. The results are areas of cancerous tissue with distances to blood vessels longer than the maximum diffusion distance of oxygen (150 µm) [45]. This, and other factors, can lead to tumour necrosis [46].

Referring to the ability of combined µCT and DLIT to detect viable, luciferase expressing tumour cells, all these aspects concerning the tumour micro environment have to be taken into account during progression starting with the infiltration with a low cell number up to a solid tumour. In the stage of a solid tumour DLIT signal does not reflect tumour load anymore. The ability to spatially detect a DLIT signal within a tumour and related to tumour volume helps to track changes in microenvironment.

2. Aim of the project

The aim of this diploma thesis was to evaluate tumour growth and dissemination of stably luciferase expressing CMT-U27 cells in immunodeficient NMRI-nu mice using combined µCT/DLIT. Further the qualification of orthotopic canine breast cancer xenograft models as adequate metastatic models for a clinical comparative oncology was tested. For this, luciferase transfected CMT-U27 cells were injected into the mammary fat pad and tumour growth and dissemination were tracked using the IVIS™ Spectrum CT. The orthotopic implantation was histologically validated. Another aim was the applicability of Amira™ Software for a precise volume measurement based on the obtained µCTs.

3. Materials and methods

3.1. Cell line and cell transduction

CMT-U27, a ductal canine mammary carcinoma cell line, was a kind gift of Prof. Eva Hellmen, Uppsala, Sweden [47]. The cells were transduced with 3rd generation of self-inactivating lentivirus expressing the fusion protein EGFP-Luc, controlled by phosphoglycerol kinase (PGK) promotor [48]. This was done by Julia Maier, PhD student in the laboratory for macromolecular cancer therapeutics, Vienna. Then the cells were sorted for luc positive cells using a BD FACSAria II cell sorter (Becton-Dickinson, Franklin Lakes, USA). They were stored at -150°C.

3.2. Cell Culture

CMT-U27 cells were thawed and then cultured in RPMI -1640 with Glutamax medium (Sigma Aldrich) and additional 10% FBS and 50µg/ml gentamicin. Cells were grown in T75cm^2 sterile flasks in a humidified atmosphere of 5% CO_2 and 95% air at 37°C (Heracell 150i CO_2 incubator, Thermo Scientific). After two times of passaging, the cells were harvested and counted with MACSQuant® Analyzer (Miltenyi Biotec GmbH, Germany).

3.3. Animals

Six female NMRI nu/nu mice (Janvier Labs, Le Genest-Saint-Isle, France) were included in the present study. They were housed within an SPF (specific pathogen free) animal facility in individually ventilated cages (Type IIL, SealSafe IVC Next Blue Line; Tecniplast; Germany) in groups of maximum five and had free access to food (ssniff® Spezialdiäten GmbH in Soest, Germany) and autoclaved water. All procedures were documented in a Lab Animal Facility Management web app (PyRAT; Scionics Computer Innovation GmbH). The local ethics committee approved all procedures, which are also in accordance with the Austrian and European law for protection of animals.

3.4. In vivo tumour model

The first step consisted of harvesting tumour cells. The medium was aspirated and the cells were washed one time with PBS (DPBS, Sigma Aldrich, Vienna, Austria). After that, TrypLE (Fisher Scientific, Vienna, Austria) was used for detaching the CMT-U27 cells of the flask's surface. After 4 min of incubation at 37°C, the cells were examined under the microscope. When the cells were fully detached fresh medium trice the amount of TrypLE was used for

stopping the detachment reaction. Then the suspension was centrifuged at 200 g for 5 min. After this, the supernatant was rejected and the cells were resuspended in PBS and counted with MACSQuant® Analyzer (Miltenyi Biotec GmbH, Germany). Finally a dilution of 3 million cells per 50 µl PBS was made.

The second step consisted of orthotopically injecting the cell suspension (under anaesthesia) through the 4th inguinal nipple into the mammary fat pad of female NMRI nu/nu mice, using a 30 G syringe. When primary or rather secondary tumours reached an uncomfortable size for the animal or showed ulceration it was surgically removed. To remove the tumour, mice were anaestetised with 5% isoflurane (Isoflurane CP 1ml/ml, CP-Pharma, Burgdorf, Germany) using an induction chamber (Combi-Vet® anaesthesia system; Rothacher Medical, Heitenried, Switzerland). Carprofen (Rimadyl 50mg/ml); Zoetis Schweiz GmbH, Zürich, Switzerland) was pre-surgically administered via subcutaneous injection for analgesia. To prevent any movement of the animal during the surgical tumour-removal, the mouse was fixed in dorsal position to the small animal surgery table (Combi-Vet® Surgery table standard with Physitemp temperature controller unit; Rothacher medical) with black tape. 7.5% iodine solution (Braunol; B.Braun Medical AG, Melsungen, Germany) was used to disinfect the skin. Using a scalpel (Aesculap BB510 scalpel blades; B.Braun), an elliptical incision through the cutis around the tumour was made. The subcutis was opened using Metzenbaum Scissors. Surgical knots were tied for the ligation of larger vessels using Novosyn™ suture (Novosyn violet 6/0; B.Braun). The tumour and surrounding mammary fat pad tissue were removed as a whole by blunt preparation. Individual button sutures were made in order to close the wound. 500 µl Glucose (5% B.Braun) were injected intraperitoneally for the animal's recovery and it was put in a seperate cage overnight. Two parts of the excised tumour were frozen and one part was kept in 70% ethanol for future processing. All procedures were conducted under the supervision of Sebastian Gehrig.

3.5. Imaging procedures

The IVIS™ SpectrumCT (Perkin Elmer), an integrated optical and µCT technology for small animal imaging in pre-clinical settings, performed bioluminescence (2D-BLI and 3D-DLIT) and computed tomography. For 2D BLI, the system's settings were adjusted to acquiring images with an open filter for maximum sensitivity. 3D DLIT was performed as follows. As a first step the system acquired a µCT scan. The second step was to generate five 2D bioluminescence surface radiance images at emission wavelengths 560, 580, 600, 620 and 640 nm using narrow bandpass filters typical for firefly luciferase. Imaging time points were individ-

ually set according to visible tumor development for each animal. Anesthesia was induced as described above. Na-Luciferin (Promega, Mannheim, Germany) was dissolved in PBS (120 mg/kg) and then injected subcutaneously. The best timepoint to start the imaging process with the IVIS™ Spectrum CT was 15 min post substrate application as this allowed for optimal diffusion of the substance. Ointment (Vit-A-POS Augensalbe; URSAPHARM Arzneimittel GmbH) was used as eye protection for the animals. Contrast agents (Scanlux, Sanochemia, Vienna; ExiTron™ nano, Miltenyi Biotec GmbH, Bergisch Gladbach, Germany; Visipaque, Ge Healthcare Buchler GmbH & Co. KG, München, Germany) were applied variably depending on the individual requirements of the animals. Mice were placed in dorsal position on the platform and the nose was put into the nose cone, where an isoflurane supply preserved anesthesia. Forearms and hind limbs were extended and attached to the platform with black tape, which prevented photon scattering. The optimal time point for BLI/DLIT was 15 min after Na-Luciferin injection and marked the beginning of the plateau phase. Initially, a 2D whole body image was acquired. This was used to estimate signal strength and signal distribution. Based on this, the DLIT settings were adjusted. The settings for the µCT were adjusted to medium resolution and for the BLI to auto exposure and a binning of 8. As a first step, the whole body of the animal was imaged in 2D. When BLI signals were detected both in thorax and abdomen, the following 3D DLIT imaging was divided into two separate imaging rounds. The field of view was then centered firstly on mid abdomen and secondly on mid thorax. After imaging procedure 500 µl Glucose (5% B.Braun) were injected intraperitoneally for animal's recovery and it was put back into its cage. Cervical dislocation was performed as euthanasia, when the animals' discomfort related to tumour growth, ulceration or other conditions reached the definite end-point criteria. In that case, final DLIT and µCT were done. Animals were then euthanized and dissected. Ex vivo 2D BLI images of tissues and organs were finally acquired.

3.6. Living Image ™ Software for image analysis and tomographic reconstruction

Living Image™ Software (Version 4.5.2., Perkin Elmer) was used for image data analysis. The reconstruction was done as follows.

Open Living Image™, select the relevant DLIT/µCT folder and open the file. Then select in the Tool Palette *Surface Topography* and click *Generate Surface*. A surface outline will be displayed in the 3D viewer. After that select *DLIT 3D Reconstruction* in the Tool Palette and

select the filters, which are to be included in the reconstruction. A minimum of three filters have to be selected. After starting the process a photon density map of the spectrally filtered BLI signals in 2D will appear in the Data Preview Window, generated out of the selected filters. These signals can be adjusted manually using the tabs at the bottom of the menu. Then click *Reconstruct* and the algorithm will start. To provide detailed anatomical localization of the 3D DLIT signal within the µCT scan, the 3D volumetric data can be adjusted in 3D Multimodality tools. For signal quantification, volumetric regions of interest (ROI) are drawn, covering individual organs, regions or tumour areas.

3.7. Amira® Software for tumour segmentation and volume measurement

Amira® Software (Version 6.4, Thermo Fisher Scientific) was used for tumour segmentation and volume measurement, following the protocol below.

Loading image data

First, image data has to be loaded. Open Amira® software and select: *Start* > *Open Data* > select the folder containing the CT data (.dicom format).

Choosing image filters

Image features can be enhanced by applying a wide range of filters for controlling contrast, smoothing, noise reduction and feature enhancement. Smoothing is the most important category for preparing data for image segmentation. A basic filter preserving edges is the Median filter.

Project view > choose your prior opened data > *Median filter* > select *3D* > *apply*.

Image Segmentation

Segmentation means assigning labels to image voxels that identify and separate objects in a 3D image. Tumour tissue was segmented in order to distinguish it from the rest of the mouse body and subsequently measure its volume.

Segmentation editor > choose as *image data* your already *filtered* data > select *materials* new > rename it to „tumour'' > switch to the 4-viewer layout by clicking on the *Four viewers* button in the *viewer toolbar* > adjust the contrast in the *Zoom and data* window.

Scroll through the slices with the scroll wheel of the computer mouse until you find the tumour. You can choose between coronal, sagittal or transversal orientation in the 4-viewer layout.

In the *Tools* area of the Segmentation Editor's main panel you can choose between different tools (e.g. brush, lasso, magic wand) for marking the tumour. The general procedure is done as follows: mark the tumour in one orientation > scroll 3 slides further and mark the tumour there > continue this procedure from one end of the tumour to the other > then press *selection* > *interpolate* > to assign the selected pixels of all slices to the material *tumour*, select it in the *Materials* list, then click the **+** *button* in the *Selection group*.

Volume measurement

Once a structure is segmented, volume measurement can be done. *Main menu* > select *Segmentation* > *Material Statistics.* A table appears in a dialog window listing amongst others the volume of each material.

Volume rendering

Project view > choose your *filtered data* > *Volren.* In the *Properties* colormap and contrast can be adjusted. In order to also show the segmented tumour in the 3D modus, combine *Volren* with your *labeled data* and then again with your *filtered data,* in order to get a triangular connection between them. Then press *Volren* > *edit*(colormap) in the *Properties* window > *materials* > *tumour.* The segmented tumour shows up.

3.8. Histology

Organs and Tissues were put for 24 hours in separate 50ml falcon tubes and filled up with formaline 4%. After fixation each sample was placed in a white plastic cassette and processed over night for 12 to 14 hours using an SLEE MTP Carousel tissue processor (SLEE medical GmbH, Mainz). The samples were then paraffin embedded using a SLEE MPS/P1 embedder (SLEE medical GmbH, Mainz). 2 µm sections were cut with a microtome (CUT 4062, SLEE medical GmbH, Mainz) and mounted on micro slides.

3.9. HE-staining

Slides were deparaffinated in a hydration row with increasing hydrophilicity. Then the slides were stained with Harris Haematoxylin solution (LOT SLBM3739V, Sigma-Aldrich®, HHS16) and Eosin Y solution (LOT # MKBQ9365V, Sigma-Aldrich®, 318906). Subsequently the slides were dehydrated in a dehydration raw with increasing lipophilicity. Slides

were finally covered with Entellan®new rapid mounting medium (LOT HX42534561, Merck) and cover slips.

3.10. Microscopy

The stained sections were analyzed with a flourescence microscope (BX53, Olympus Life Science). The additional camera (DP72, Olympus) was used for taking pictures of the sections.

4. Results

Three million CMT-U27 cells in 50 µl PBS was orthotopically injected (under anesthesia) through the 4th inguinal nipple into the mammary fat pad of every of the six female nude mice. Sebastian Gehrig performed the injection, due to his veterinarian education. A primary tumour grew in the mammary fat pad of every animal, validated by histology (Fig.1).

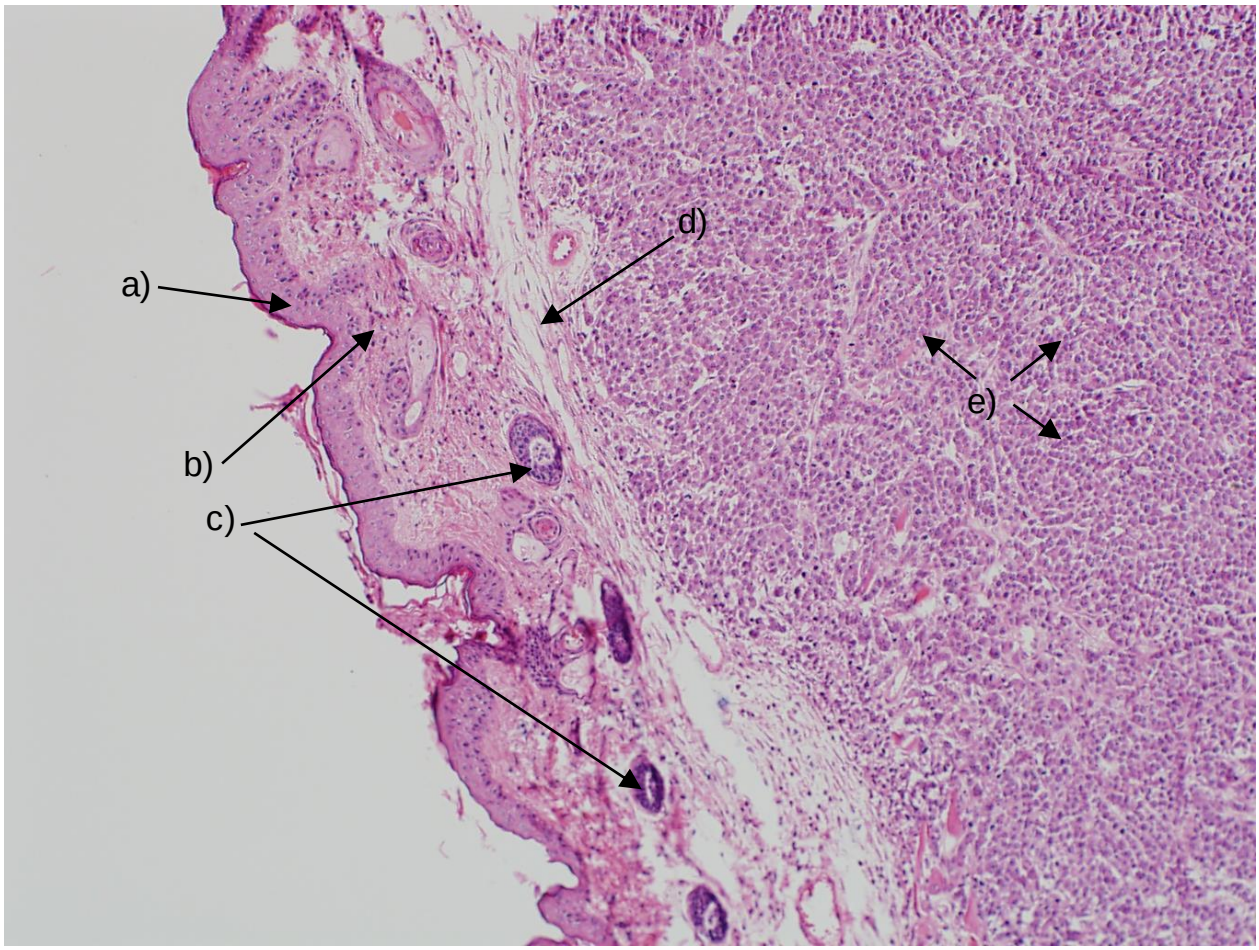

Fig.1: Example of a primary tumour growing in the mammary fat pad after orthotopic implantation of CMT-U27 tumour cells. a) epidermis b) dermis c) mammary gland d) fat tissue e) primary tumour.

4.1. Animal 90

Due to very slow tumour growth, primary tumour associated DLIT signal increased from 2,98E+07 ph/sec directly following implantation to 9,39E+10 ph/sec 111 days later. Signals were located at the rim of the primary tumour indicating viable, luciferase expressing tumour cells, while the core of the tumour was without DLIT signal (Fig.2a,b). Subsequently on day 111 the primary tumour was excised due to tumour size (Fig.2d) showing a volume of 992 mm^2 (Fig.2c). Post-surgery imaging showed in the region of the right axillary lymph node a signal of 4,59E+06 ph/sec (Fig.4).

39 and 57 days later further imaging was done, showing DLIT signal increase of metastatic lesions in the region of the right axillary lymph node, the right inguinal lymph node and the skin. The signals 39 days after tumour removal were separately reconstructed, in order to also detect weaker DLIT signals (Fig.5a,c). On day 57 separate reconstruction was not necessary, due to a sufficient increase (Fig.5b,d). The tumour nodules were also surgically removed on day 57 (Fig.7a,c). The skin lesion showed a volume of 610 mm^3 (Fig.7b).

Two weeks after the second surgery the animal was euthanized because of severe sickness. The following dissection showed tumour growth in the area of the right axillary and inguinal lymphnode (Fig.8). The lymphnodes were removed for cell isolation in order to generate a more aggressive CMT-U27 sub-line.

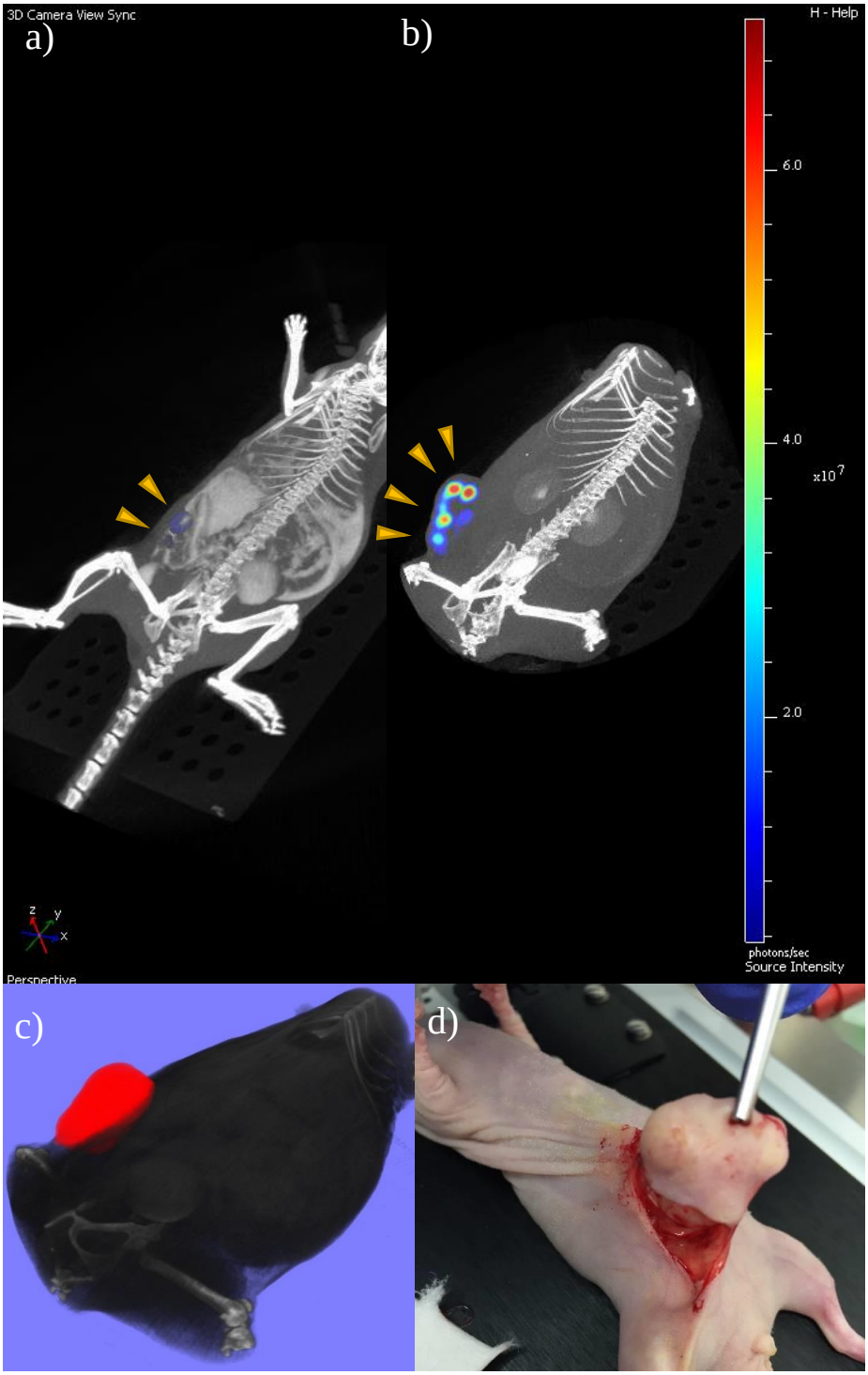

Fig.2: a) DLIT signal strength and distribution on day 0, directly after the implantation of the cell suspension into the mammary fat pad. b) DLIT signal strength and distribution of the solid primary tumour growing in the mammary fat pad on day 111 post implantation. a) and b) are using the same equalized colour scale indicating the signal strength in photons/sec and yellow arrows indicating the signal distribution. c) tumour segmentation and volume measurement using Amira™ software; V=992 mm^3. d) surgical removal of the primary tumour on day 111. The tumour was located in the mammary fat pad of the animal which proved the successful orthotopic implantation of the CMT-U27 cells.

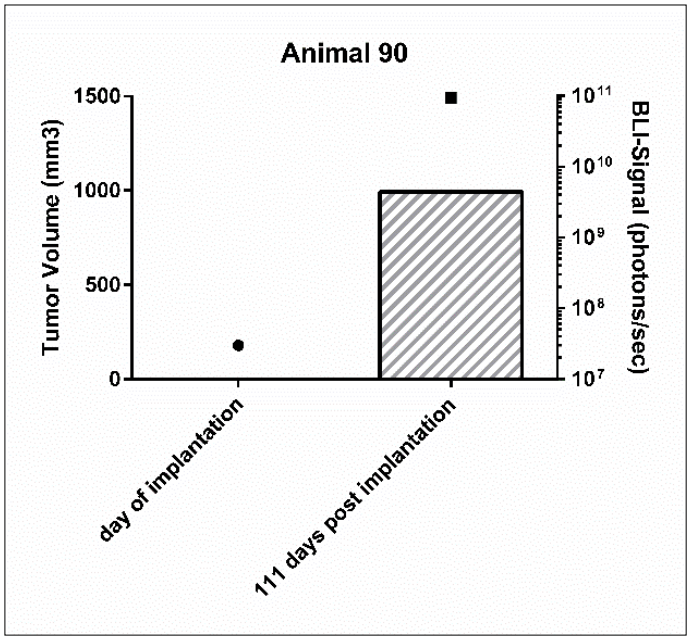

Fig.3: Total increase of the DLIT signal in relation to primary tumour growth. The dots are indicating the DLIT signal in photons/sec and the columns are indicating the tumour volume in mm^3.

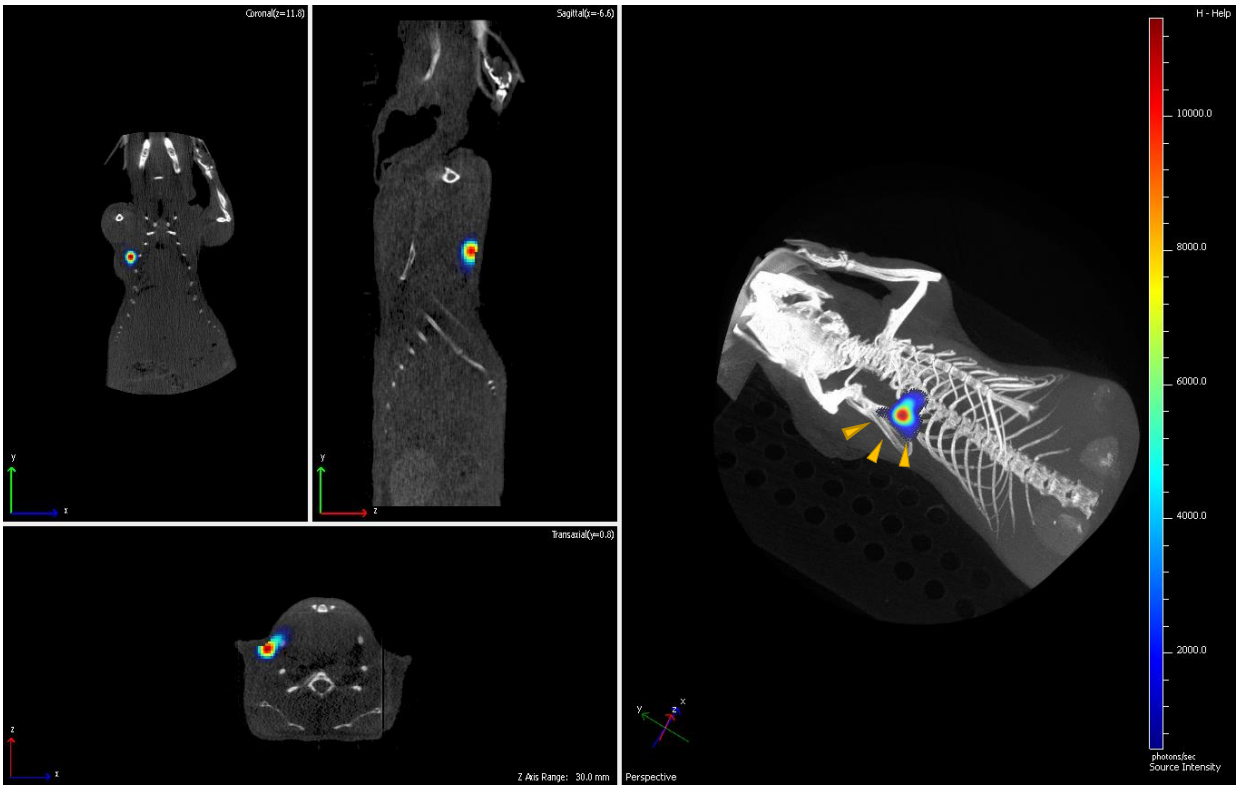

Fig.4: Metastatic lesion in the region of the right axillary lymph node directly after removal of the primary tumour on day 111, indicated by yellow arrows.

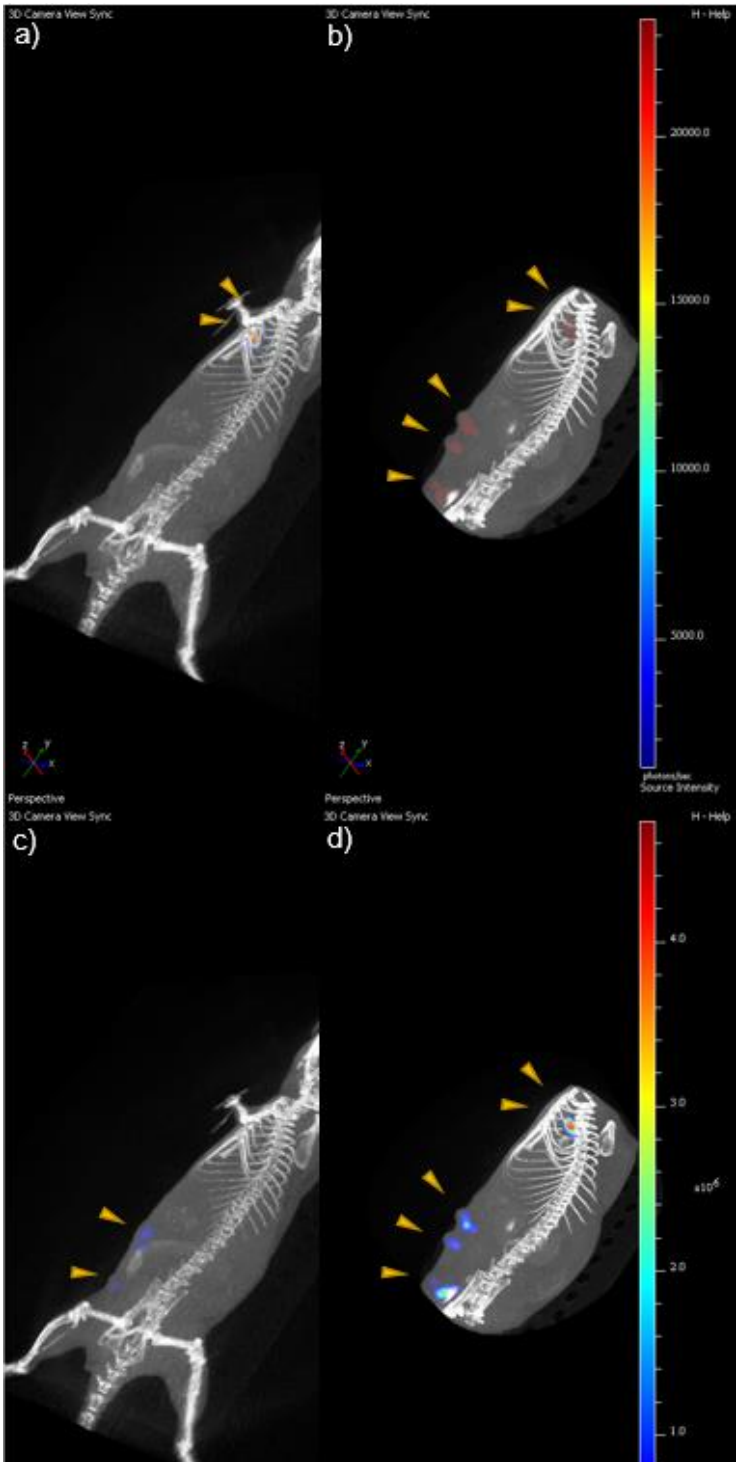

Fig.5: a) DLIT signal of the right axillary lymph node 39 days after excision of the primary tumour. c) DLIT signal of the skin lesion and the right inguinal lymph node at the same time point. b,d) same signals 57 days post-surgery. a,b) and c,d) are using the same equalized colour scale indicating the signal strength in photons/sec and yellow arrows indicating the signal distribution.

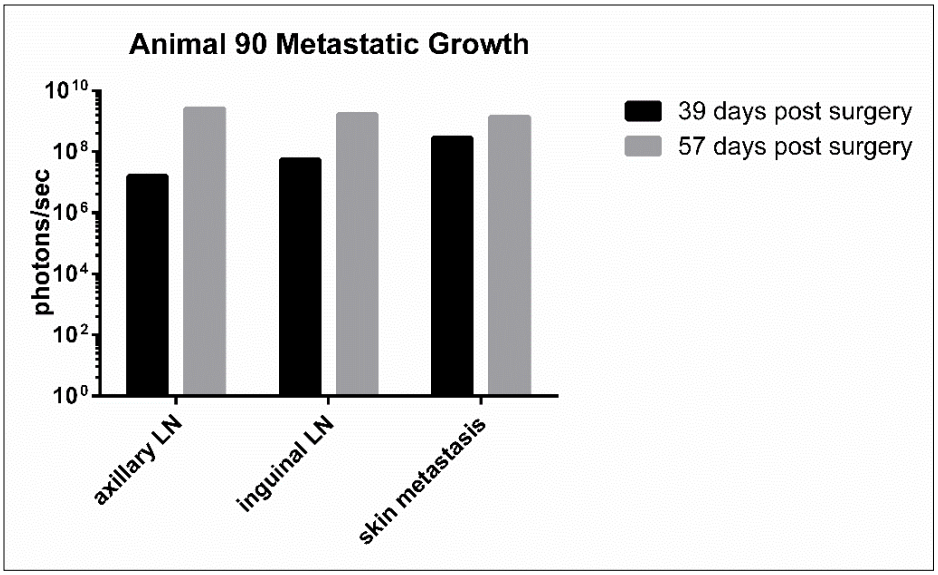

Fig.6: Increase of the DLIT signal 39 and 57 days after the removal of the primary tumour.

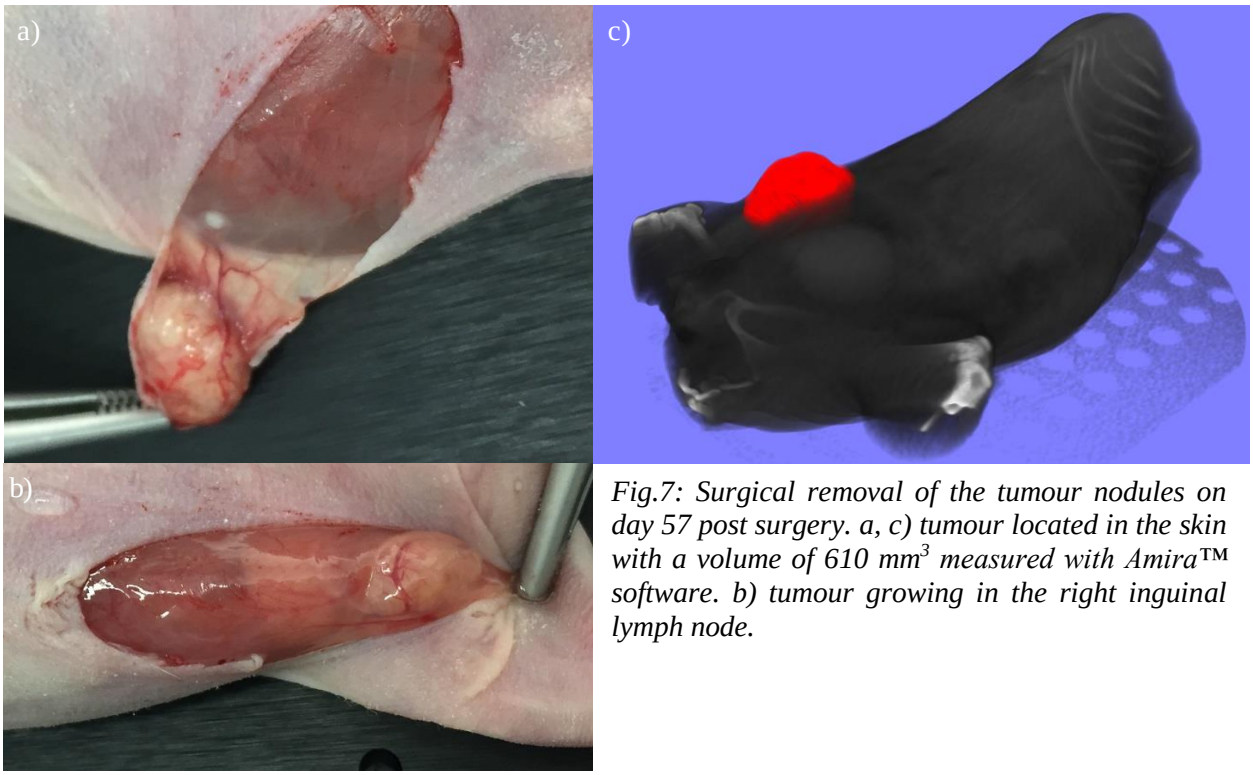

Fig.7: Surgical removal of the tumour nodules on day 57 post surgery. a, c) tumour located in the skin with a volume of 610 mm^3 measured with Amira™ software. b) tumour growing in the right inguinal lymph node.

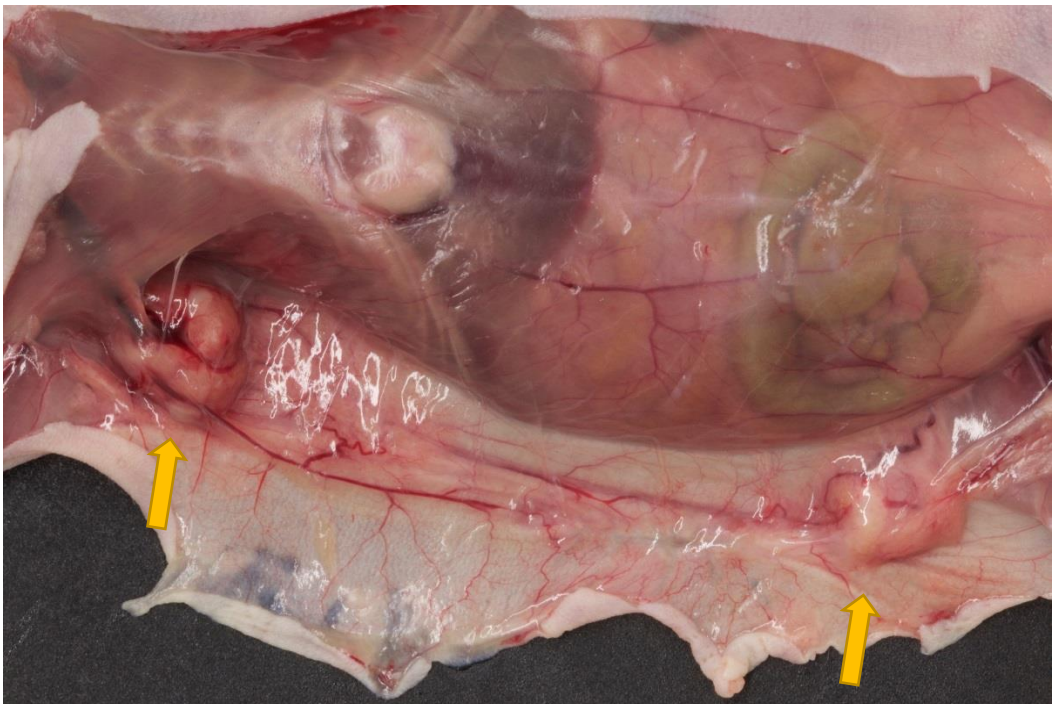

Fig.8: The final dissection two weeks after the second surgery showed tumour growth in the area of the right axillary and inguinal lymphnode (indicated by yellow arrows).

Animal 91

Animal 91 was imaged in total three times. Tumour associated DLIT signal increased to 1,34E+11 ph/sec in a timeframe of 40 days (Fig.9a,b). 20 and 40 days post implantation primary tumours were segmentated and volume was measured using Amira™ software showing volumes of 107 mm^3 and 1113 mm^3 (Fig.9d,e). The DLIT to volume ratio 20 days post implantation showed a value of 4,68E+08 ph/sec/mm^3. 40 days post implantation the ratio decreased to 1,20E+08 ph/sec/mm^3 due to changes in the tumour microenvironment during tumour growth, for example necrosis, hypoxia or insufficient access to the substrate (Fig.10). Also the distribution of DLIT signal within the primary tumour showed signal free areas in the core and viable light emitting cells at the rim (Fig.9c). After primary tumour excision 40 days post implantation (Fig.11) no more radiologic or clinical evidence of tumour burden was found.

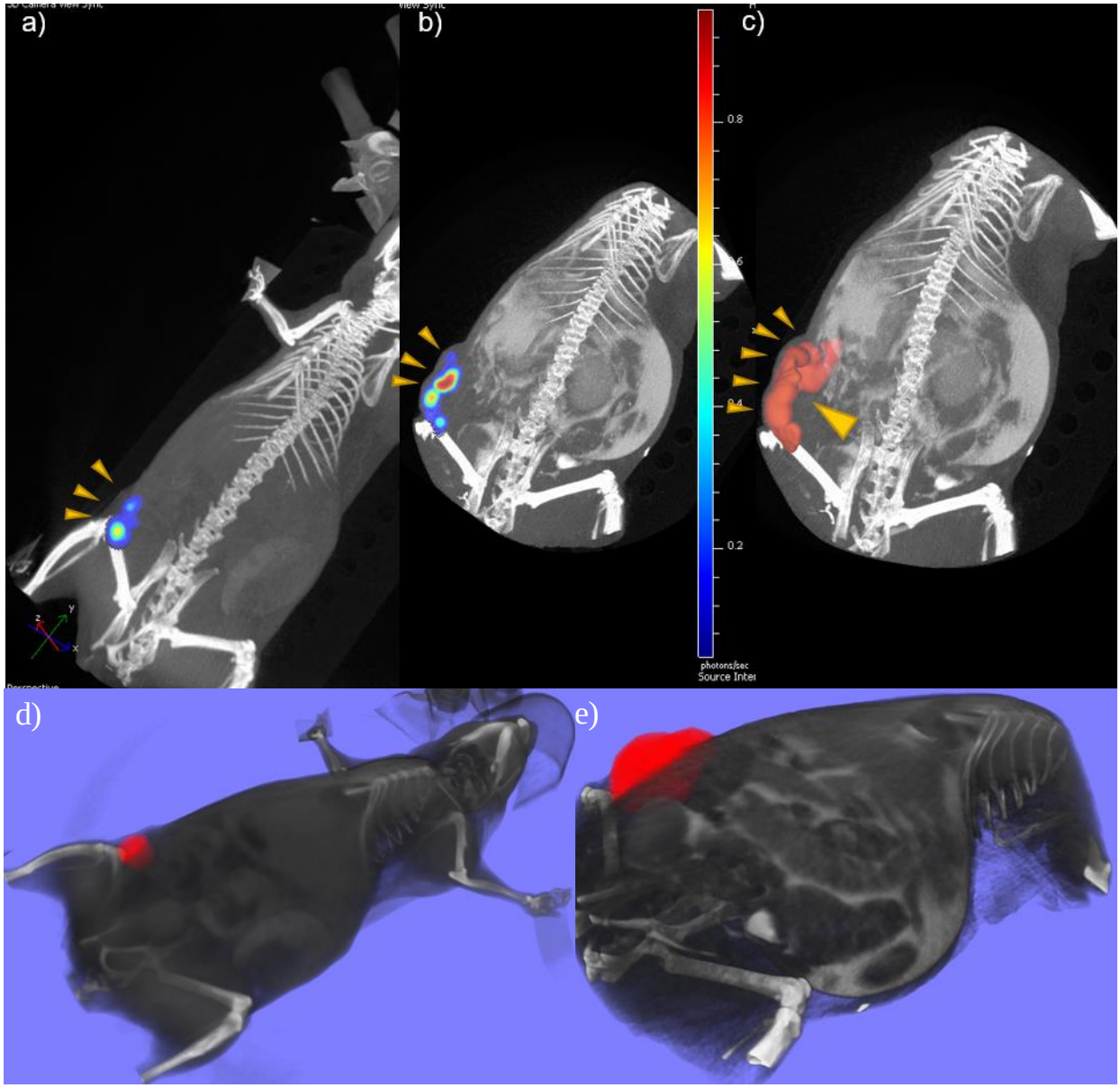

Fig.9: Optical increase of the DLIT signal, DLIT signal distribution and tumour segmentation and volume measurement.
a) Primary tumour growing in the mammary fat pad 20 days post implantation of 3 million CMT-U27 cells. b) Primary tumour growing in the mammary fat pad 40 days post implantation. a,b) are using the same equalized colour scale indicating the signal strength in photons/sec and yellow arrows indicating the signal distribution. c) The isosurface of the reconstructed source volume demonstrates the three dimensional distribution of the DLIT signal at the rim of the tumour and a signal free area in the core of the tumour 40 days post implantation (indicated by yellow arrows).
d,e) tumour size 20 (V=107 mm^3) and 40 days post implantation (V=1113 mm^3).

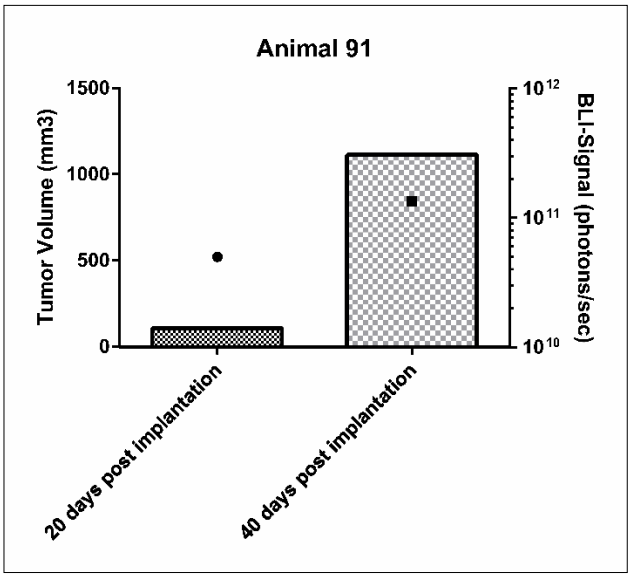

Fig.10: Total increase of the DLIT signal in relation to primary tumour growth in a timeframe of 40 days. The dots are indicating the DLIT signal in photons/sec and the columns are indicating the tumour volume in mm^3.

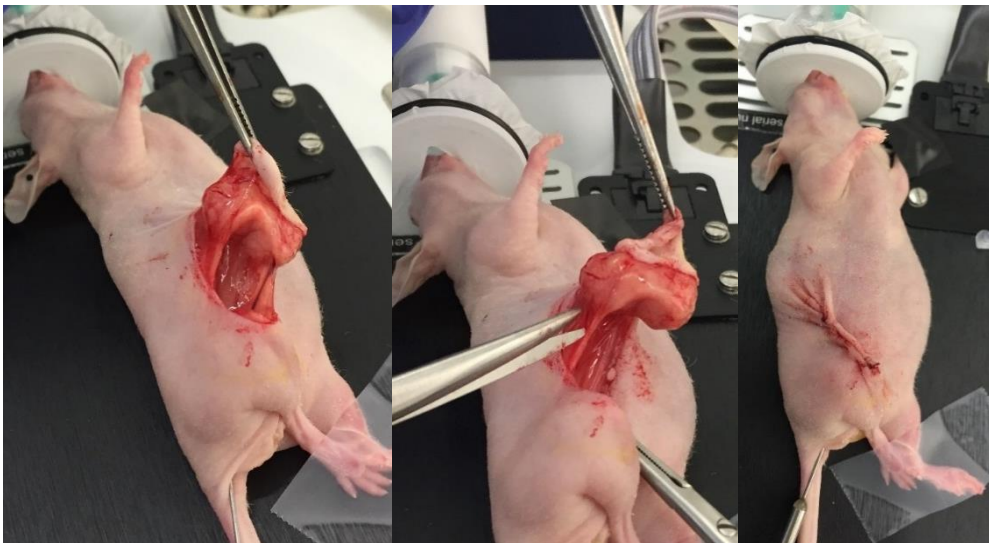

Fig.11: Surgical removal of the primary tumour due to tumour size 40 days post implantation.

Animal 92

Animal 92 was imaged three times. Tumour associated DLIT signal increased to 5,00E+10 ph/sec (Fig.12) in a timeframe of 33 days. Also the distribution of DLIT signal within the primary tumour showed signal free areas in the core and viable light emitting cells on the rim (Fig.13). Comparing the DLIT/volume ratio 20 days post implantation (4,84E+07 ph/sec/mm^3) with the ratio 33 days post implantation (4,35E+07 ph/sec/mm^3) a decrease of the ratio is indicated due to changes in the tumour microenvironment during tumour growth (Fig.15). On day 33 post implantation primary tumour, with a volume of 1150 mm^3, was excised (Fig.14). Directly after tumour removal the animal was once again imaged in 2D. The area of the sutured wound showed BLI signals (Fig.16). The animal died after surgery.

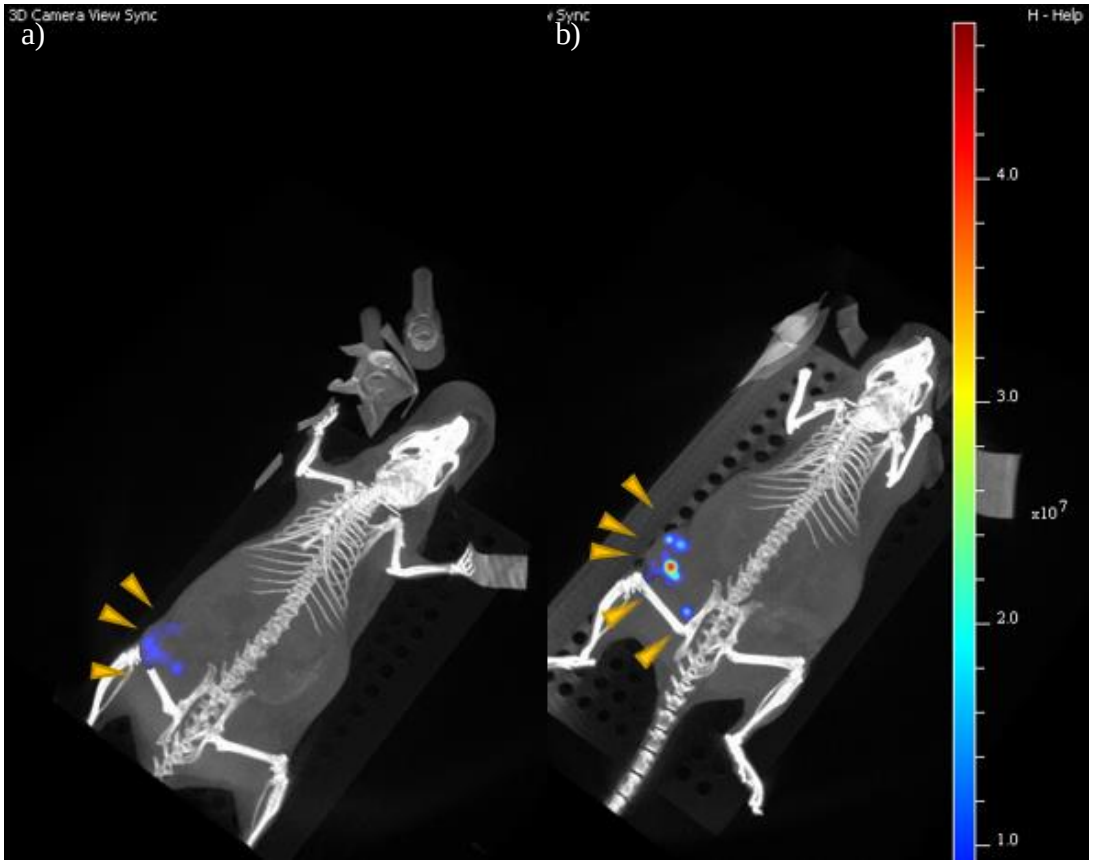

Fig. 12: Optical increase of the DLIT signal and DLIT signal distribution.
a) Primary tumour growing in the mammary fat pad 20 days post implantation of 3 million CMT-U27 cells. b) Primary tumour growing in the mammary fat pad 33 days post implantation. a,b) are using the same equalized colour scale indicating the signal strength in photons/sec and yellow arrows indicating the signal distribution.

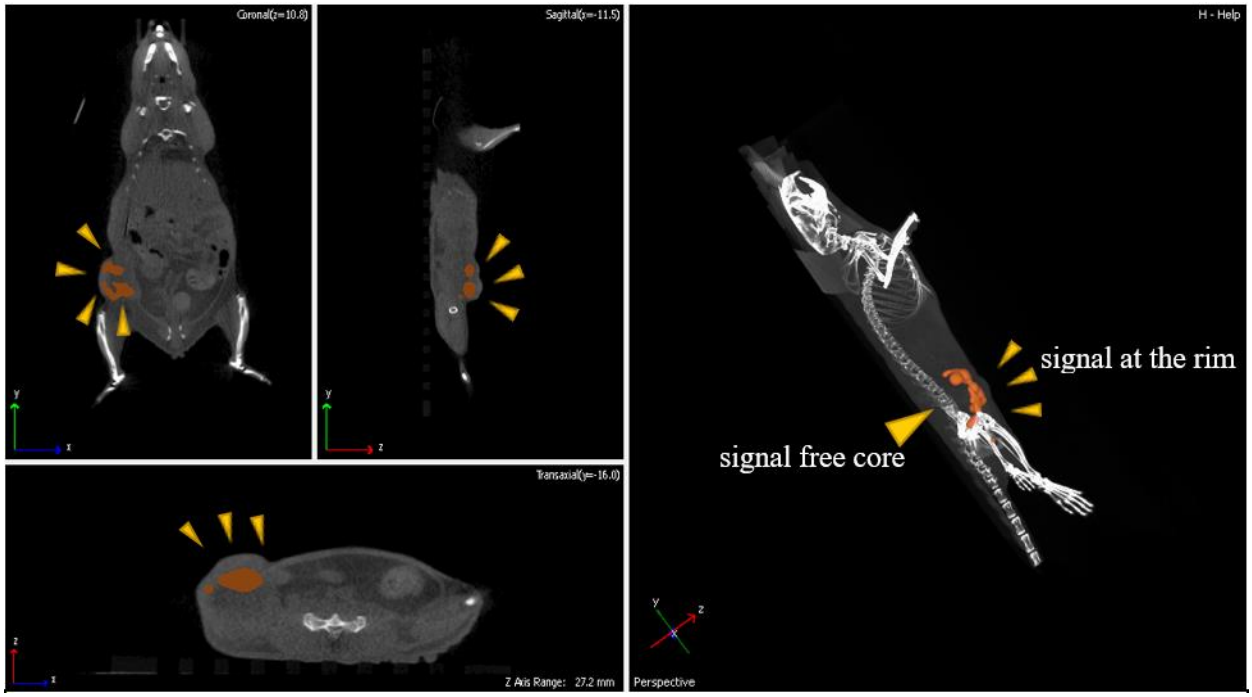

Fig. 13: The isosurface of the reconstructed source volume demonstrates the three dimensional distribution of the DLIT signal within primary tumour volume indicating its microenvironment. Again the signal is mainly located at the rim of the tumour next to a signal free area in the core which can be put down to the fact of a necrosis or other changes in the tumour micro environment.

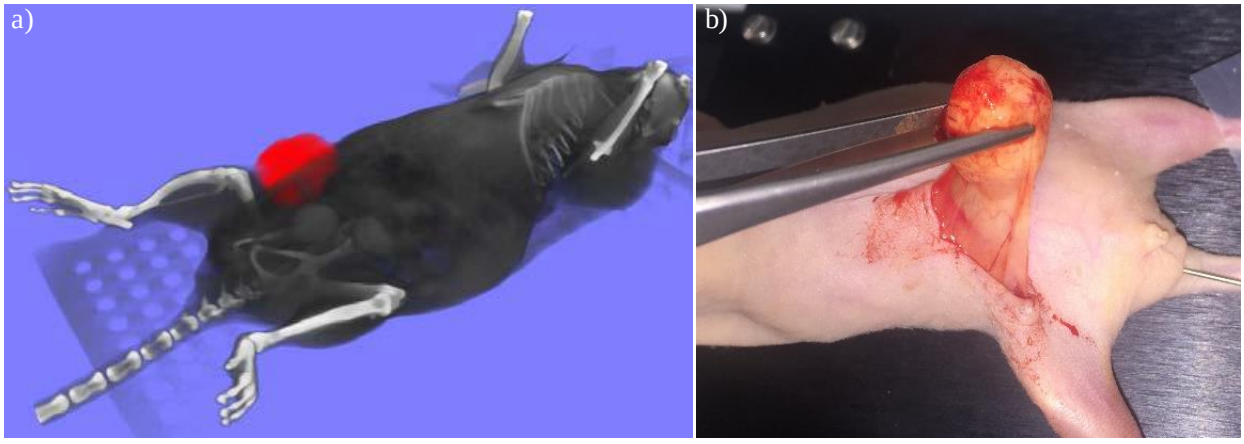

Fig. 14: a) tumour segmentation and volume measurement using Amira™ software on day 33 post implantation. V = 1150mm^3. b) excision of the primary tumour located in the mammary fat pad on day 33 post implantation.

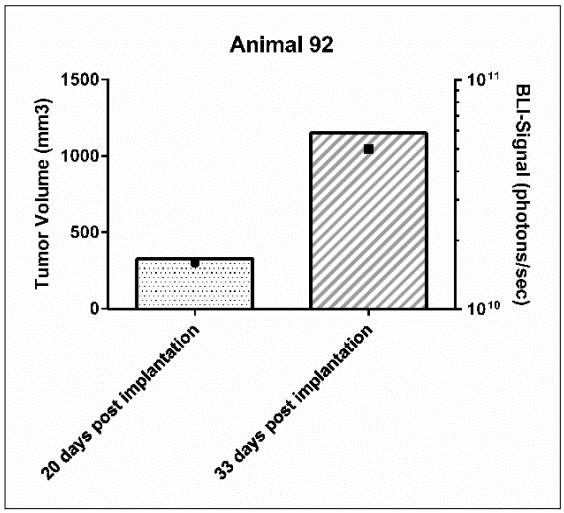

Fig.15: total increase of the DLIT signal in relation to primary tumour growth in a timeframe of 33 days. The dots are indicating the DLIT signal in photons/sec and the columns are indicating the tumour volume in mm^3.

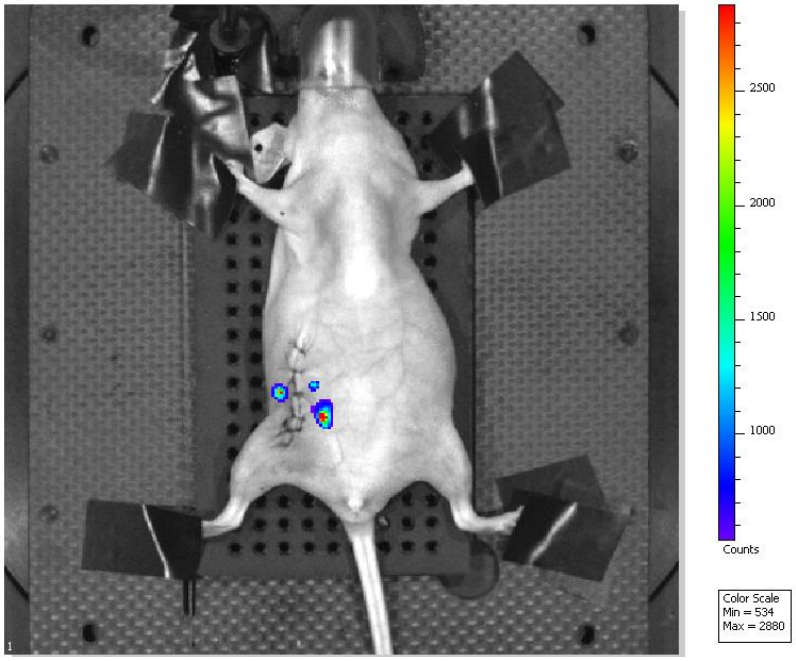

Fig. 16: BLI signals directly post surgery in the area of the satured wound.

Animal 93

Animal 93 was imaged three times until surgery. Tumour associated DLIT signal increased to 1,28E+11 ph/sec in a timeframe of 55 days (Fig.18). Also the distribution of DLIT signal within the primary tumour showed signal free areas in the core and viable light emitting cells at the rim (Fig.19) Initially tumour volume and DLIT signal grew proportionally, but then DLIT signal with respect to tumour volume decreased indicating a decrease of viable tumor cells within the whole tumour volume (Fig.17). Tumour size increased to a volume of 842 mm^3 (Fig.18f). After primary tumour excision 55 days post implantation a metastatic lesion grew in a timeframe of 49 days to a solid secondary tumour. In this frame the animal was imaged at three additional time spots (Fig.20). Again the tumour showed the same signal distribution patterns as before in the primary tumour (Fig.21). The tumour microenvironment again changed from a proportional DLIT/volume increase to a later stagnating DLIT signal relatively to tumour volume (Fig.22). Due to its size the secondary tumour was excised (Fig.23) with a volume of 506 mm^3 (Fig.20d). Directly after the surgery, the animal was once again imaged showing three small signals in the area of the former secondary tumour, which could possibly be related to a metastatic process (Fig.24). The signals did not show up at the next time point of imaging. The animal was apparently tumour-free.

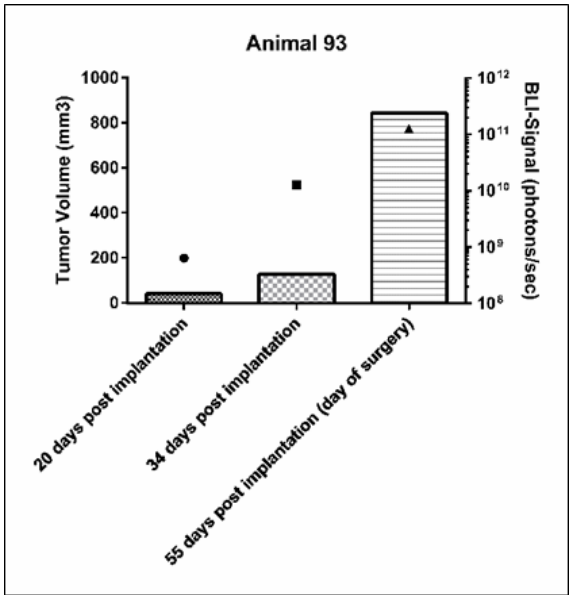

Fig.17: total increase of the DLIT signal in relation to primary tumour growth in a timeframe of 55 days. The dots are indicating the DLIT signal in photons/sec and the columns are indicating the tumour volume in mm^3.

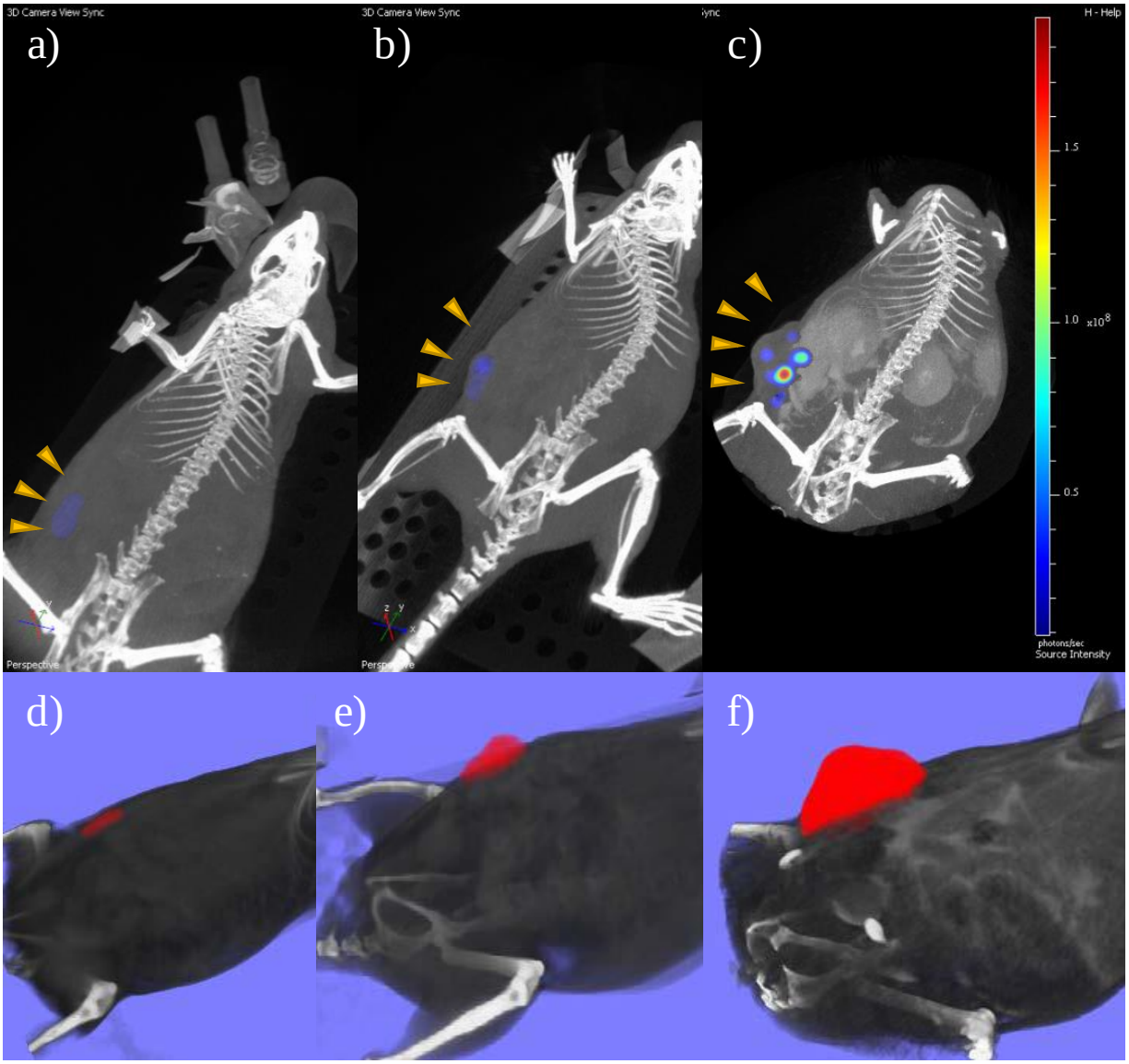

Fig. 18: Optical increase of the DLIT signal, DLIT signal distribution and tumour segmentation and volume measurement.
a) Primary tumour growing in the mammary fat pad 20 days post implantation of 3 million CMT-U27 cells. b) Primary tumour growing in the mammary fat pad 34 days post implantation. c) Primary tumour 55 days post implantation; day of surgery a,b,c) are using the same equalized colour scale indicating the signal strength in photons/sec and yellow arrows indicating the signal distribution. d,e,f) tumour size 20 (V=40 mm^3) and 34 (V=127 mm^3) and 55 days post implantation (V=842 mm^3).

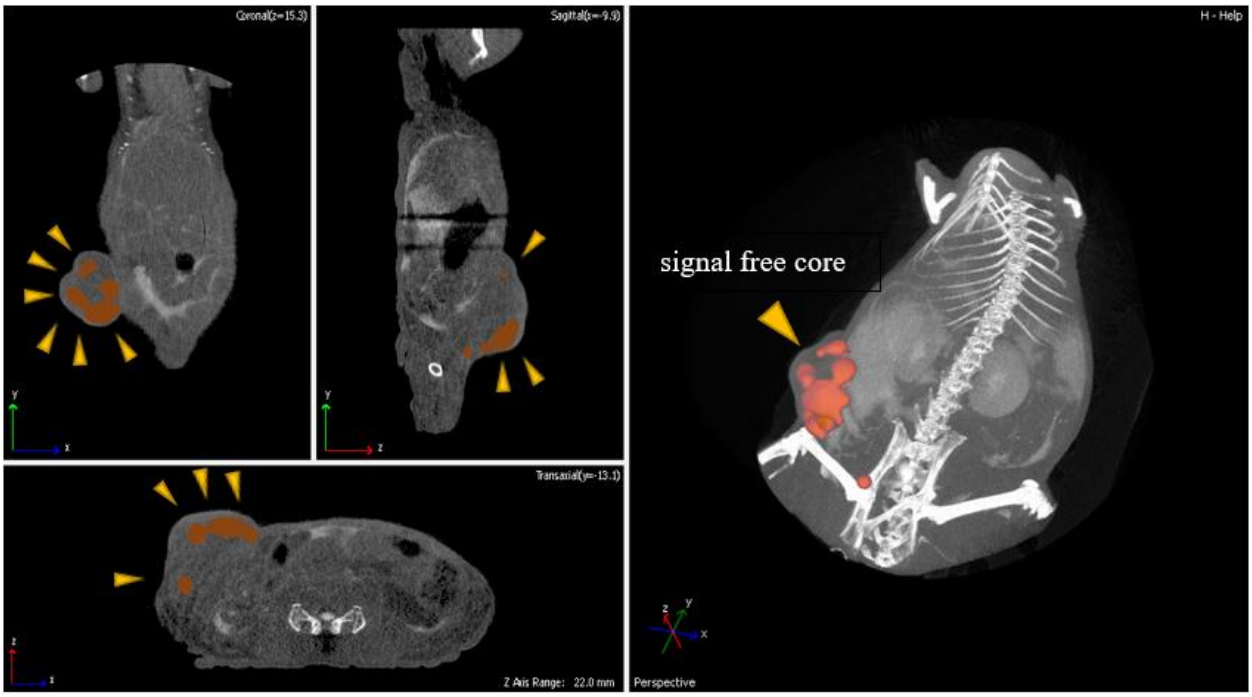

Fig. 19: The isosurface of the reconstructed source volume on day 55 post implantation demonstrates the three dimensional distribution of the DLIT signal within primary tumour volume indicating its microenvironment. The signal is mainly located at the rim of the tumour next to a signal free area in the core which can be put down to the fact of a necrosis or other changes in the tumour microenvironment.

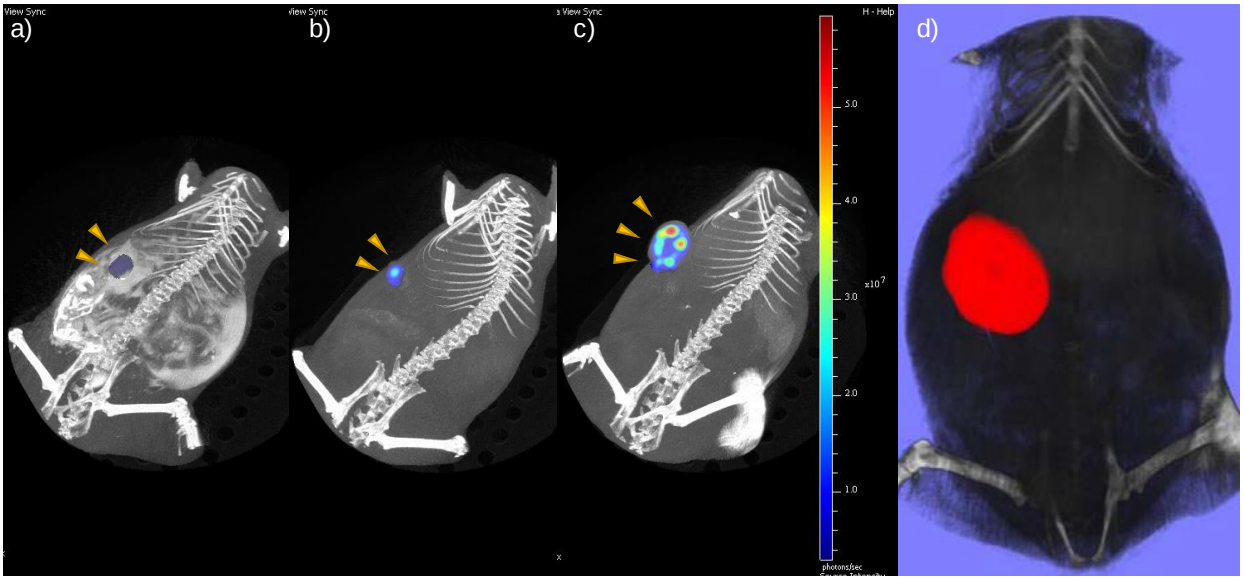

Fig. 20: Optical increase of the DLIT signal, DLIT signal distribution and tumour segmentation and volume measurement.
a) Secondary tumour 12 days post surgery. b) Secondary tumour 29 days post surgery. c) Secondary tumour 49 days post surgery; day of the second surgery a,b,c) are using the same equalized colour scale indicating the signal strength in photons/sec and yellow arrows indicating the signal distribution. d) tumour size of the secondary tumour 49 days post surgery (V=506 mm^3).

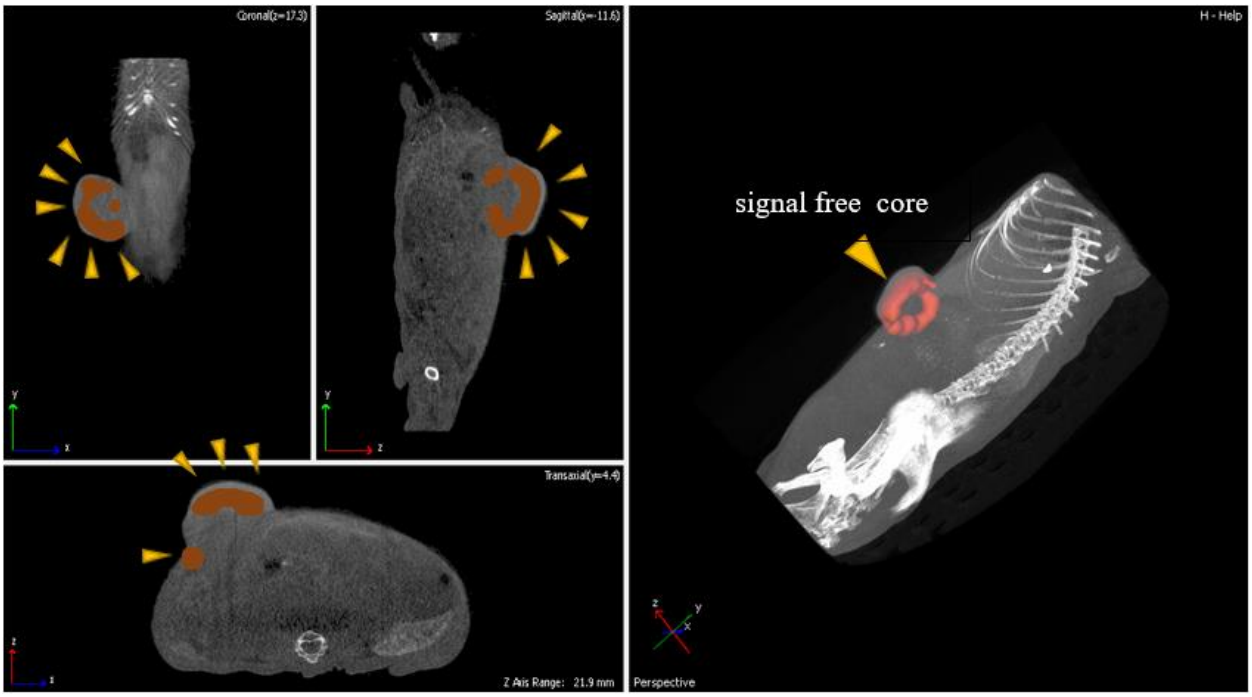

Fig. 21: The isosurface of the reconstructed source volume on day 49 post surgery demonstrates the three dimensional distribution of the DLIT signal within secondary tumour volume indicating its micro-environment. Again the signal is mainly located at the rim of the tumour next to a signal free area in the core.

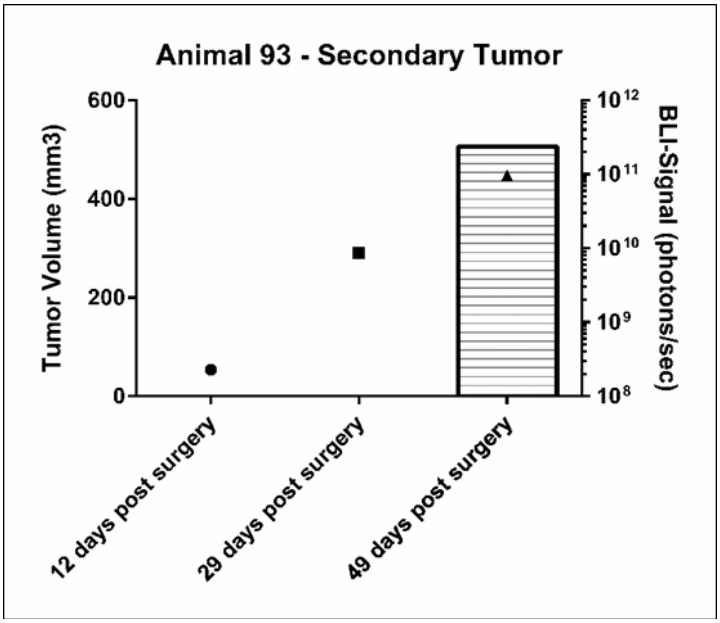

Fig.22: total increase of the DLIT signal in relation to secondary tumour growth in a timeframe of 49 days. The dots are indicating the DLIT signal in photons/sec and the columns are indicating the tumour volume in mm^3.

Fig.23: Surgical removal of the secondary tumour on day 49 post surgery.

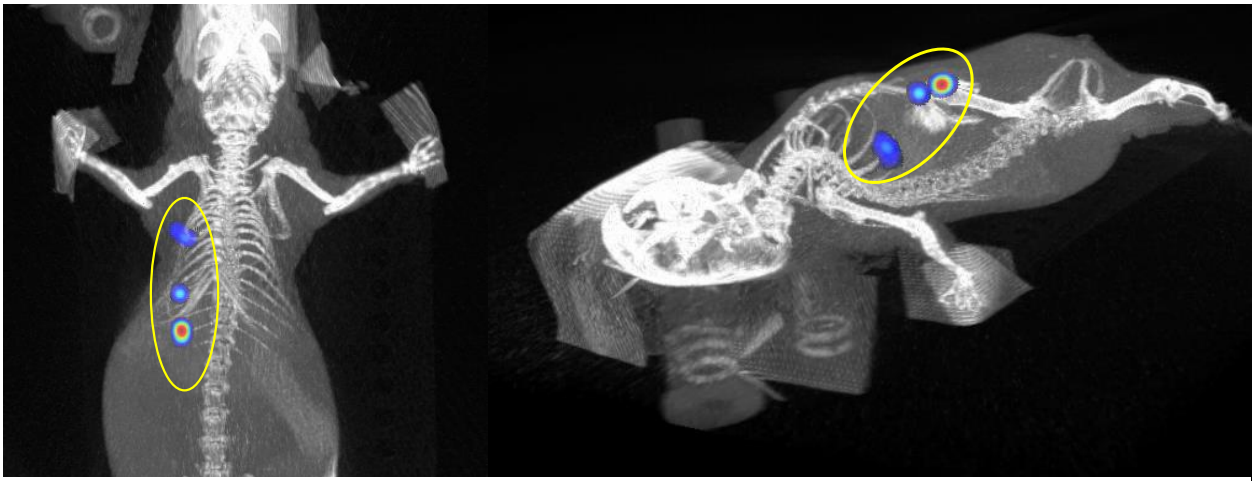

Fig. 24: Three DLIT spots in the area of the excised secondary tumour directly after the surgery.

Animal 94

In animal 94 the primary tumour was imaged twice. Tumour associated DLIT signal increased to 4,75E+10 ph/sec in a timeframe of 33 days (Fig.25). DLIT signal increased proportionally to tumour volume (Fig.26). Tumour size increased to a volume of 151 mm^3 (Fig.25d).

After primary tumour excision, the animal war again imaged at three time points (14, 34, 57 days post surgery). Secondary tumour associated DLIT signal increased to 3,63E+10 ph/sec (Fig.27). Comparing the DLIT signals of surgery one (4,75E+10 ph/sec) with surgery two (3,63E+10 ph/sec), there is no significant difference between them. But when comparing the DLIT/volume ratios there is in fact a difference between surgery one (3,15E+08 ph/sec/mm^3) and surgery two (7,67E+07 ph/sec/mm^3). The DLIT signal remained unchanged over time during secondary tumour growth (Fig.29). Also the distribution of DLIT signal within the secondary tumour showed signal free areas in the core and viable light emitting cells on the rim (Fig.28).

37 days after the second surgery (Fig.30a,b), muscle associated intraabdominal metastasis was detected with a volume of 80 mm^3 (Fig.30c,d).

The animal was imaged again 83 days after excision of the secondary tumor (Fig.31a,b). Again the tumour showed the same signal distribution patterns as before in the secondary tumour (Fig.31c,d). The muscle associated metastasis grew to a volume of 880 mm^3 (Fig. 31e). In addition to that two more metastases were detected, one on the abdominal skin and another in the left inguinal lymphnode.

After that the animal was euthanized and dissected. Tumour nodules in the area of the left inguinal lymphnode and the abdominal muscle gave proof of the metastatic process and validated the generated BLI data (Fig.32).

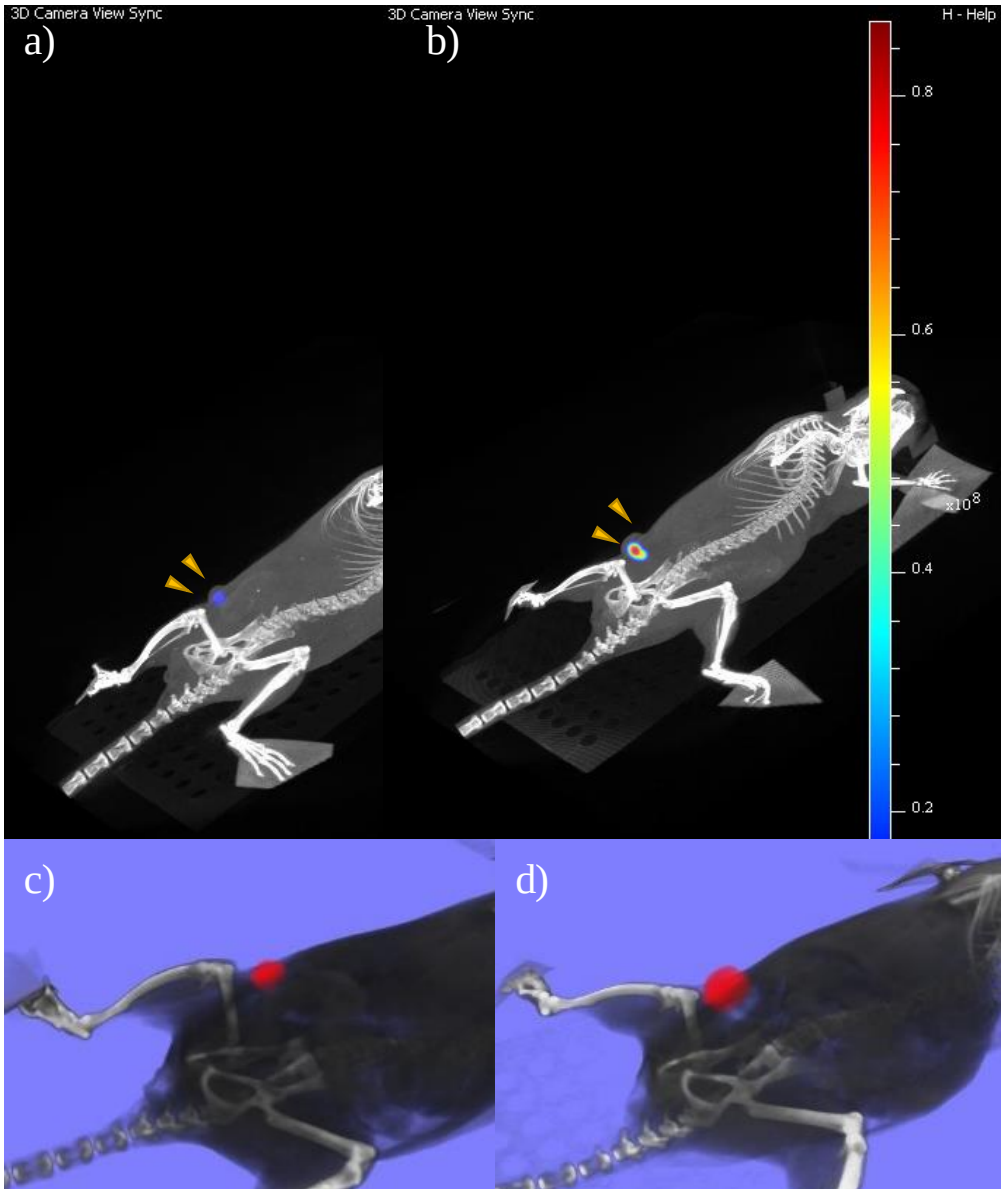

Fig. 25: Optical increase of the DLIT signal, DLIT signal distribution and tumour segmentation and volume measurement.
a) Primary tumour growing in the mammary fat pad 20 days post implantation of 3 million CMT-U27 cells. b) Primary tumour growing in the mammary fat pad 33 days post implantation; day of surgery. a,b) are using the same equalized colour scale indicating the signal strength in photons/sec and yellow arrows indicating the signal distribution. c,d) tumour size 20 (V=50 mm^3) and 33 (V=151 mm^3) days post implantation.

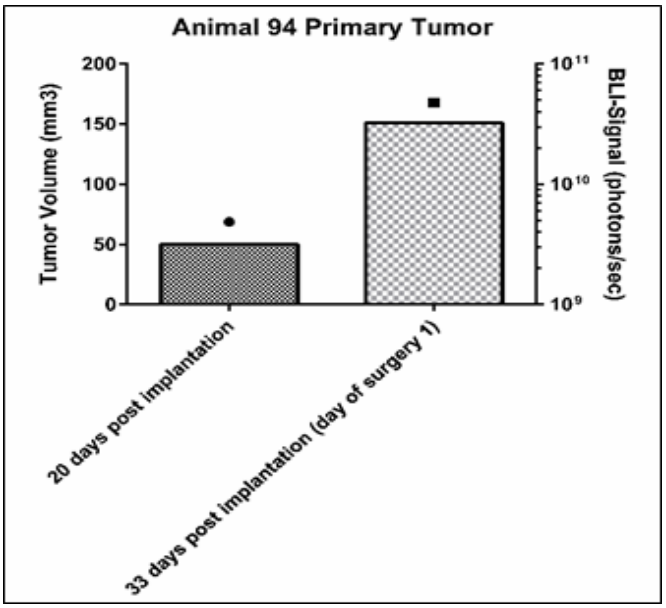

Fig.26: total increase of the DLIT signal in relation to primary tumour growth in a timeframe of 33 days. The dots are indicating the DLIT signal in photons/sec and the columns are indicating the tumour volume in mm^3.

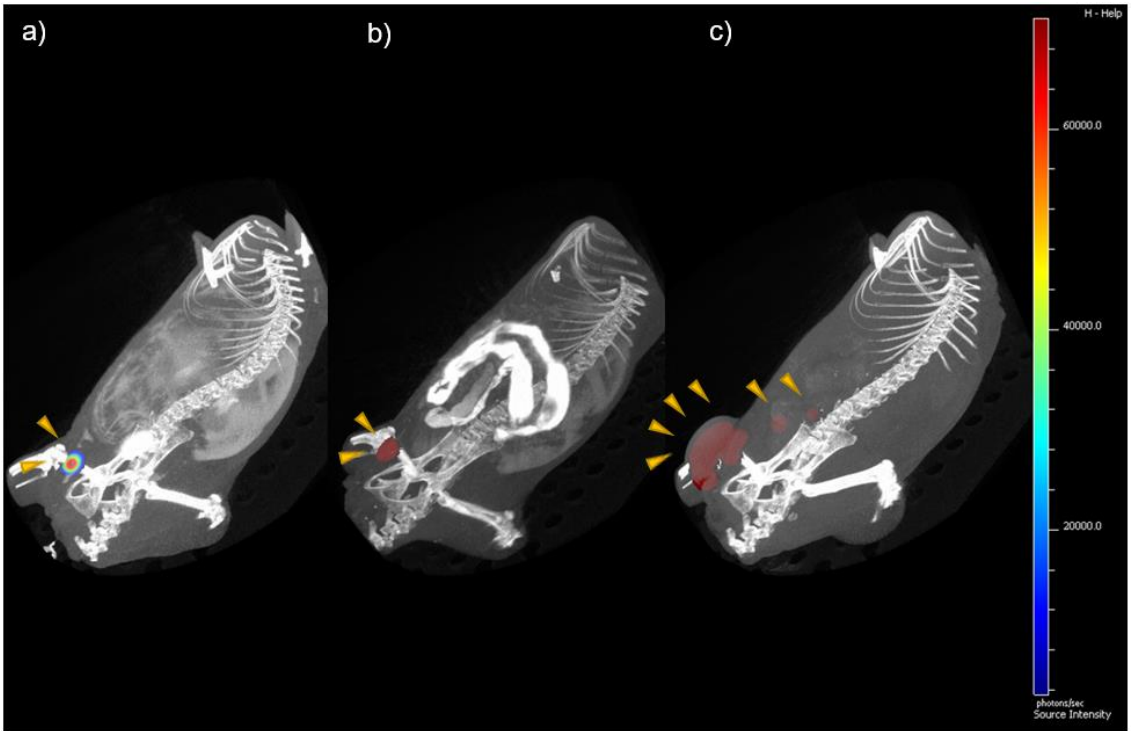

Fig. 27: Optical increase of the DLIT signal and DLIT signal distribution of the secondary tumour. a) Secondary tumour 14 days post surgery. b) Secondary tumour 34 days post surgery. c) Secondary tumour 57 days post surgery; day of surgery 2. a,b,c) are using the same equalized colour scale indicating the signal strength in photons/sec and yellow arrows indicating the signal distribution.

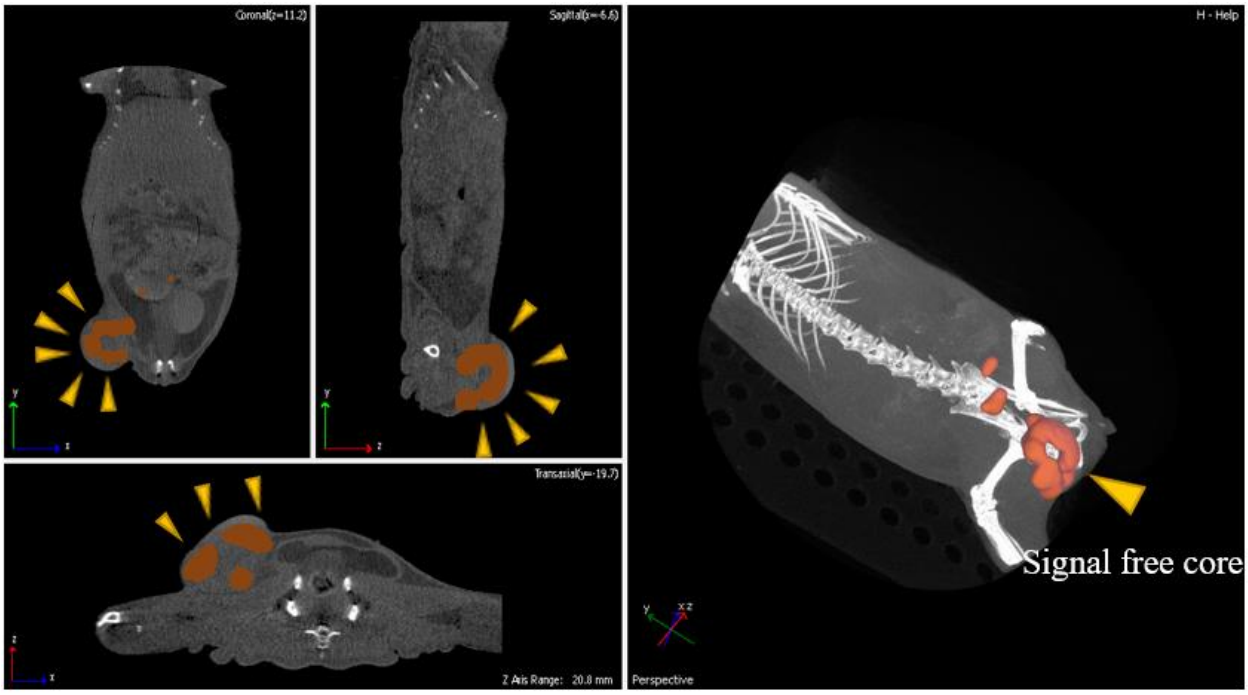

Fig. 28: The isosurface of the reconstructed source volume on day 49 post surgery demonstrates the three dimensional distribution of the DLIT signal within secondary tumour volume indicating its micro-environment. Again the signal is mainly located at the rim of the tumour next to a signal free area in the core.

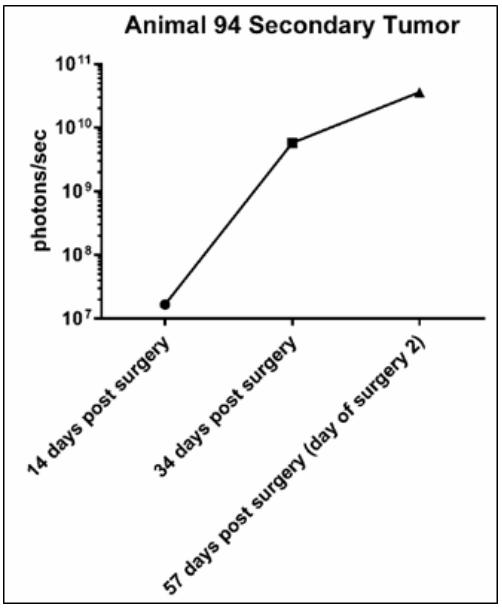

Fig.29: total increase of the DLIT signal in relation to secondary tumour growth in a timeframe of 57 days. The dots are indicating the DLIT signal in photons/sec.

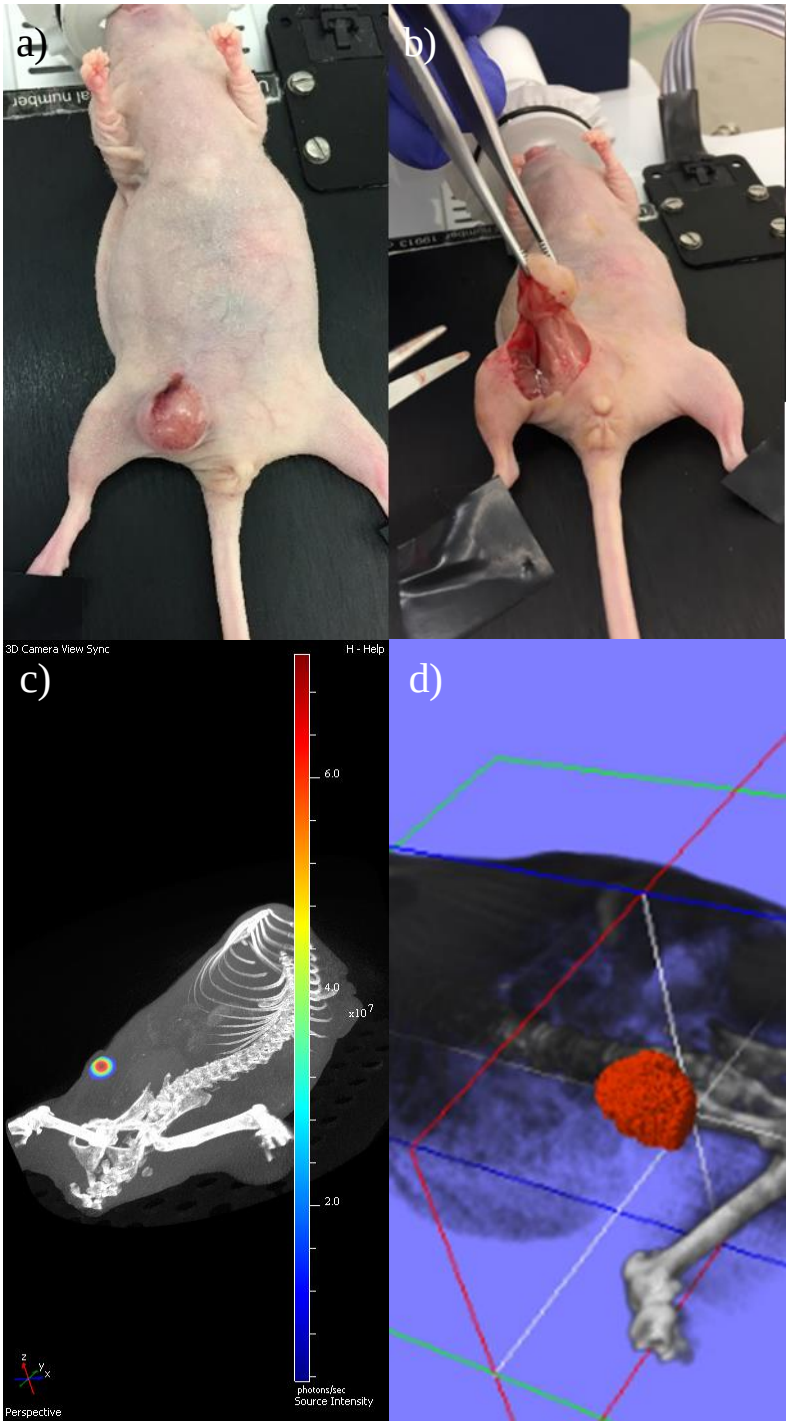

Fig.30: Surgery 2 and follow up imaging 37 days later. a,b) excision of the secondary tumour 57 days post surgery 1. c,d) muscle associated intraabdominal metastasis (V=80 mm^3) 37 days post surgery 2..

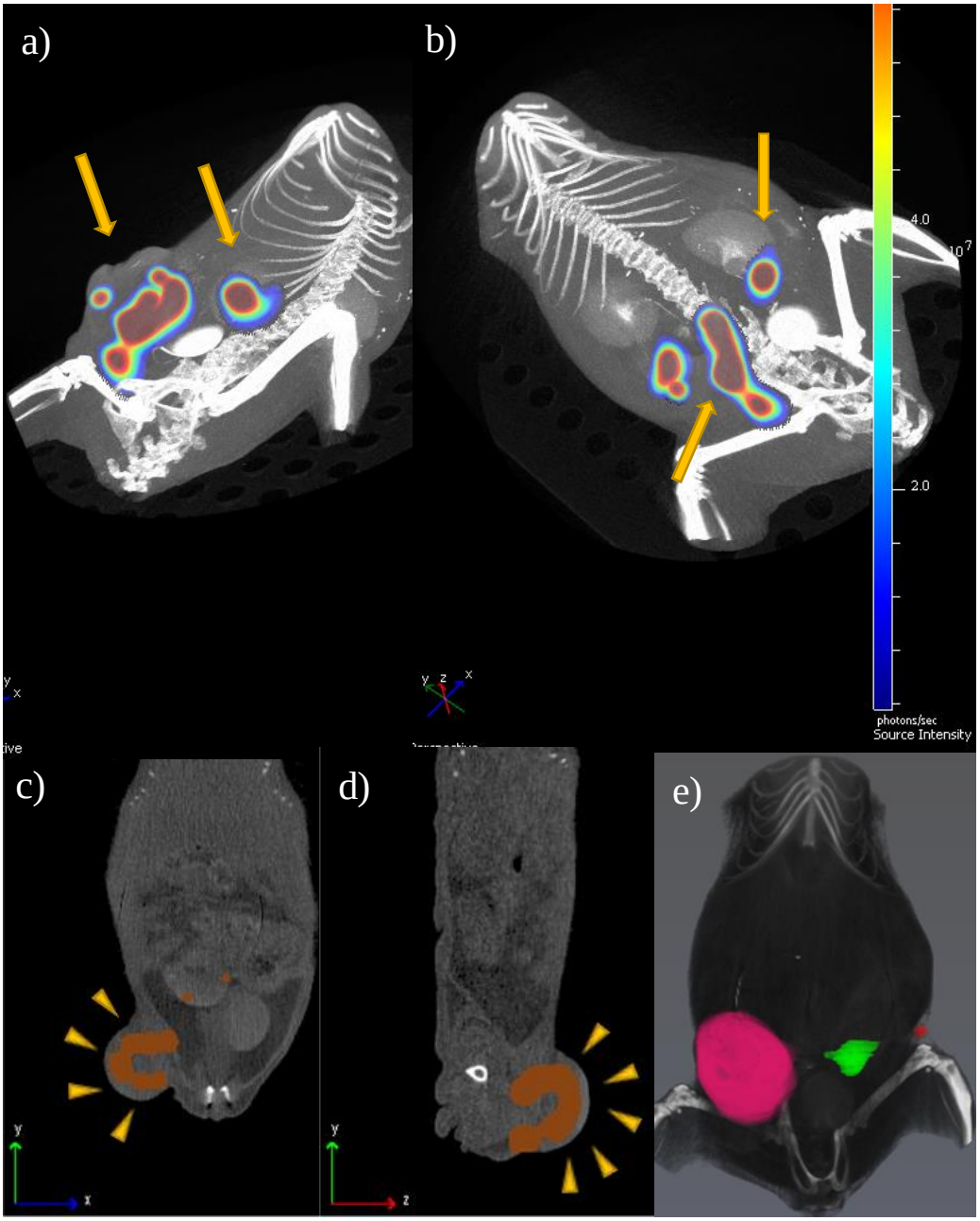

Fig. 31: Optical increase of the DLIT signal, DLIT signal distribution and tumour segmentation of the muscle associated metastasis, the metastasis in the abdominal skin and the metastasis in the left inguinal lymphnode. a,b) DLIT signal 83 days post surgery (same equalized colour scale indicating the signal strength in photons/sec and yellow arrows indicating the signal distribution). c) coronal and d) saggital views of the distribution of the DLIT signal within secondary tumour volume indicating its microenvironment. Again the signal is mainly located at the rim of the tumour next to a signal free area in the core. e) tumour segmentation using Amira™ software: muscle associated metastasis (pink) with a volume of 880 mm3, metastasis in the abdominal skin (green) and metastasis in the left inguinal lymphnode (red).

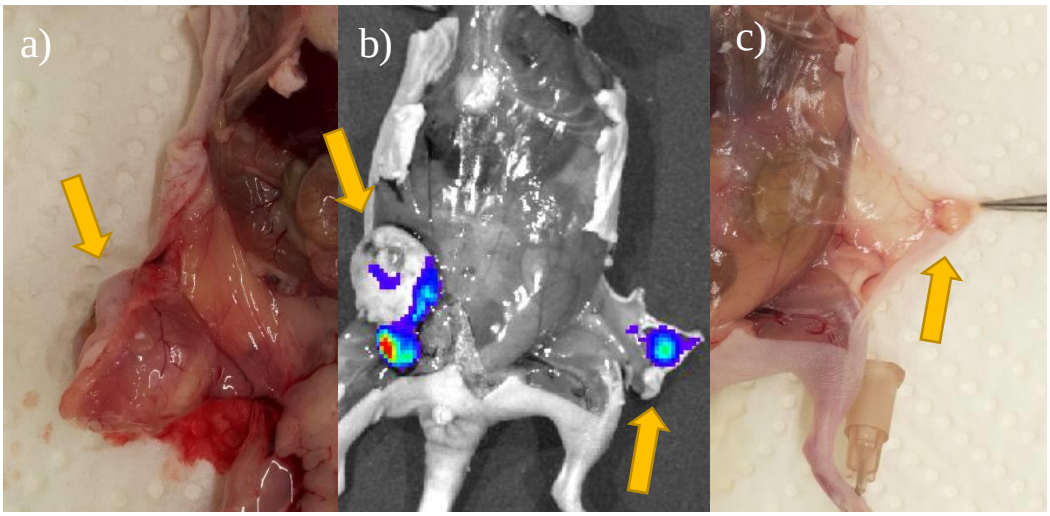

Fig.32: Dissection and final imaging post mortem. a,c) The dissection showes tumour nodules associated to the left inguinal lymphnode and the abdominal muscle (indicated by yellow arrows). b) The open body was imaged and shows BLI signals at the same spots (indicated by yellow arrows).

Animal 95

Animal 95 was imaged four times. Tumour associated DLIT signal increased to 1,16E+11 ph/sec in a timeframe of 88 days (Fig.33). Signals were located at the rim of the primary tumour indicating viable cells, while the core of the tumour was signal free (Fig.34). Subsequently on day 88 the primary tumour was excised due to tumour size showing a volume of 1119 mm^3 (Fig.33h). Initially tumour volume and DLIT signal grew proportionally, but then DLIT signal with respect to tumour volume decreased indicating a decrease of viable tumor cells within the whole tumour volume (Fig.35). 37 days after the surgery, the animal was again imaged showing DLIT signals in the area of the abdominal muscle and the skin (Fig.37a) with a total nodule volume of 144 mm3 (Fig.36b). The animal died spontaneously.

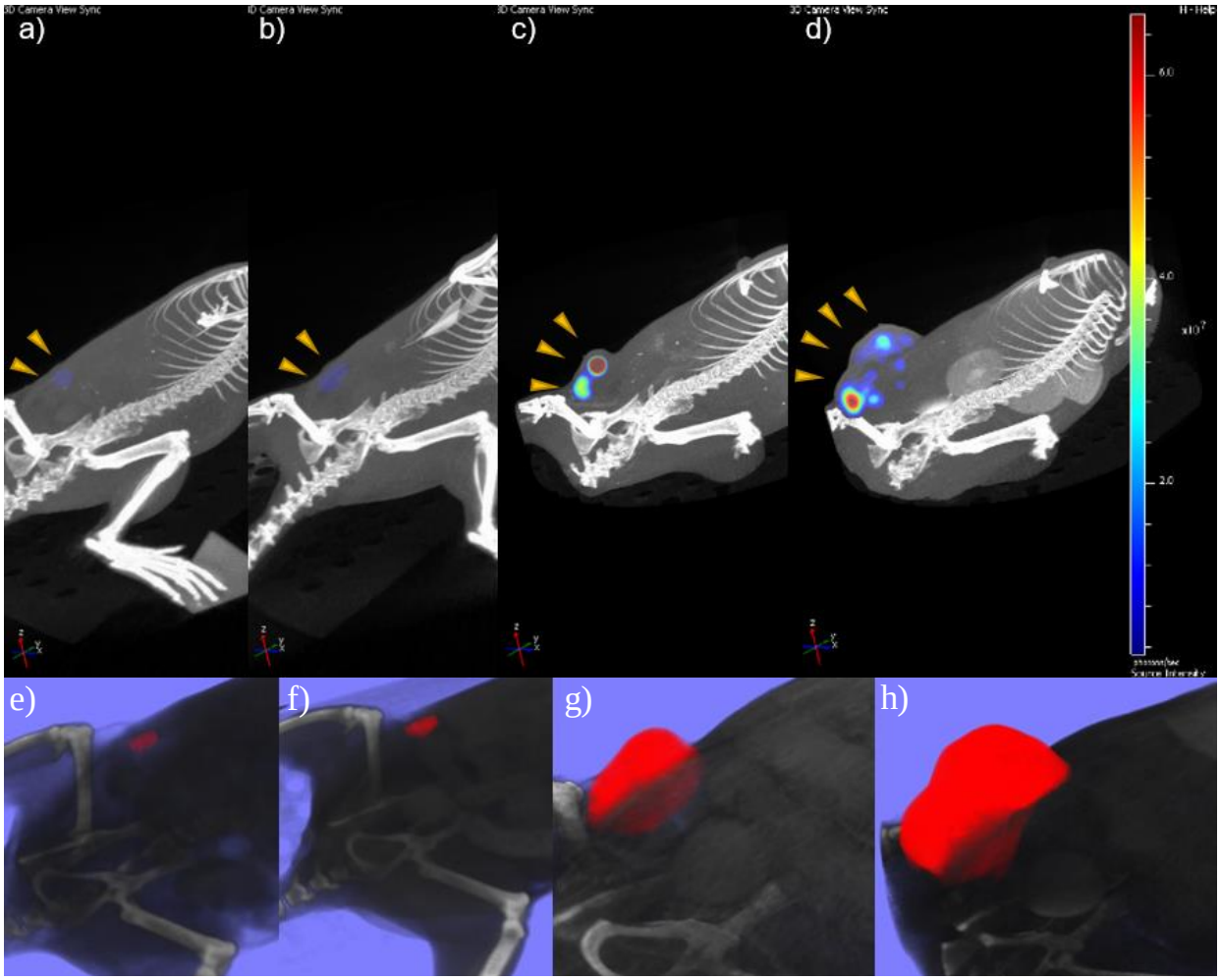

Fig. 33: Optical increase of the DLIT signal, DLIT signal distribution and tumour segmentation and volume measurement.
a, e) Primary tumour growing in the mammary fat pad 20 days post implantation of 3 million CMT-U27 cells (V=8 mm^3). b,f) Primary tumour growing in the mammary fat pad 34 days post implantation (V=16 mm^3). c,g) Primary tumour growing in the mammary fat pad 67 days post implantation (V=213 mm^3). d,h) Primary tumour growing in the mammary fat pad 88 days post implantation (V=1119 mm^3) a,b,c,d) are using the same equalized colour scale indicating the signal strength in photons/sec and yellow arrows indicating the signal distribution.

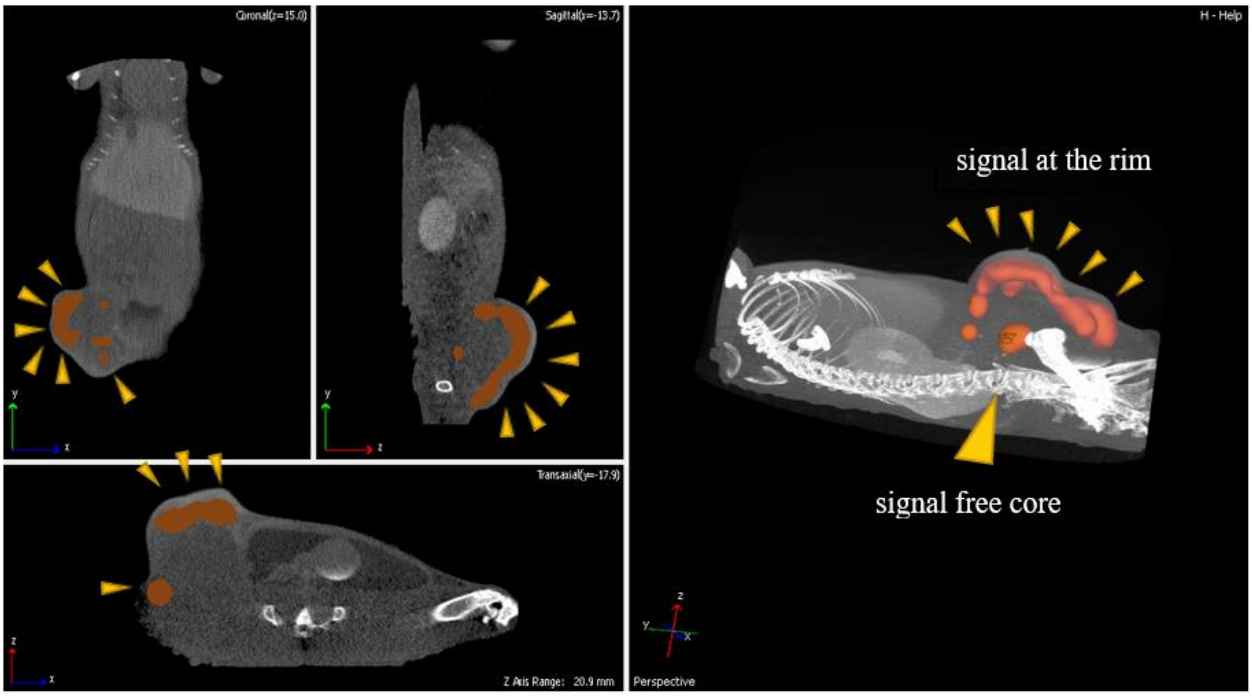

Fig. 34: The isosurface of the reconstructed source volume on day 88 post implantation demonstrates the three dimensional distribution of the DLIT signal within primary tumour volume indicating its microenvironment. The signal is mainly located at the rim of the tumour next to a signal free area in the core.

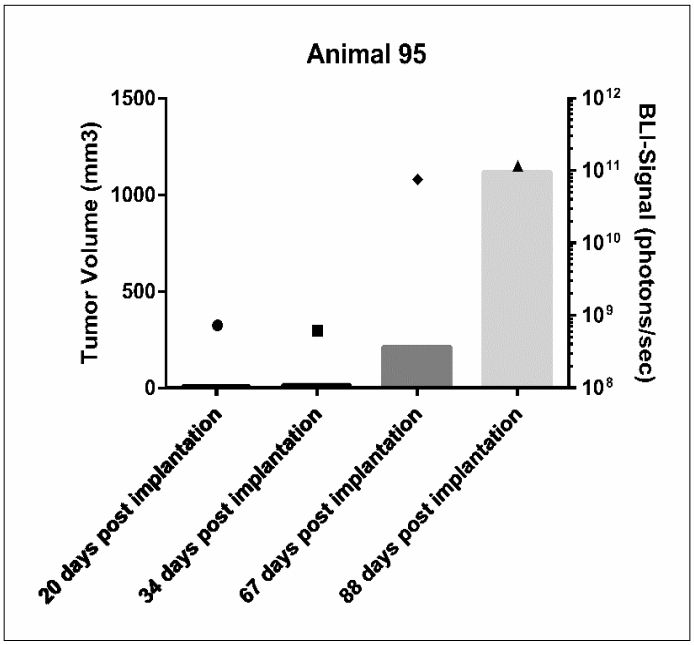

Fig.35 total increase of the DLIT signal in relation to primary tumour growth in a timeframe of 88 days. The dots are indicating the DLIT signal in photons/sec and the columns are indicating the tumour volume in mm^3.

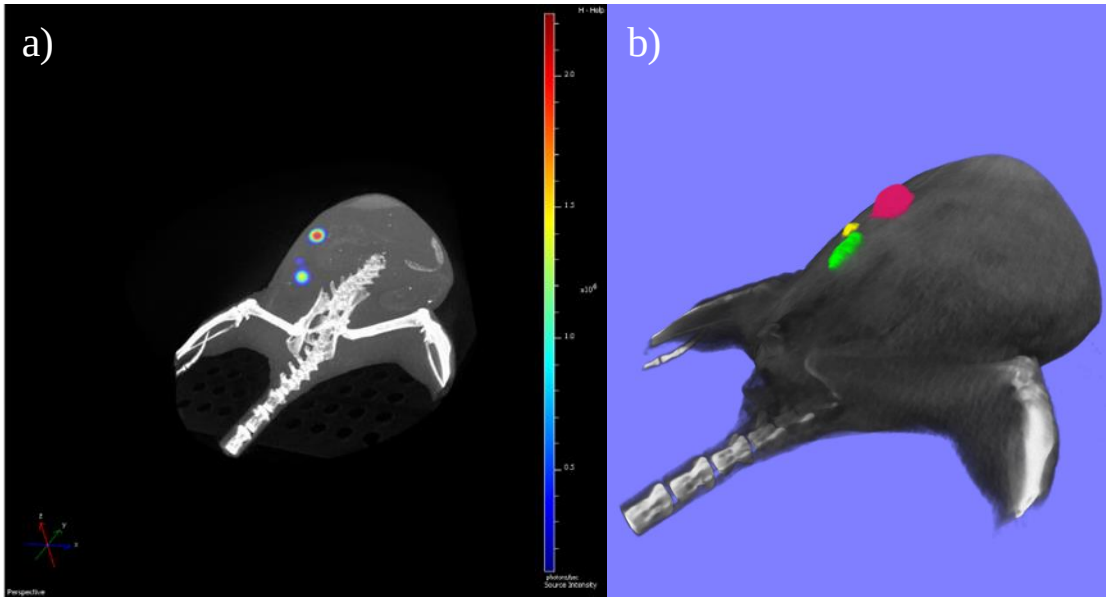

Fig. 36: a) DLIT signal 37 days after primary tumour removal. b) segmentation and volume measurement of the tumour nodules, 37 days post surgery (V=144 mm^3)

5. Discussion

Based on the studies of Weigelt and Sleecx [1, 2] we tried to establish an imageable spontaneously metastasizing canine breast cancer tumour model. The combination of DLIT and µCT allowed for longitudinal and real time visualization of tumour growth, beginning with the orthotopically injected tumour cells till the formation of solid tumours. Every experimental animal was examined individually. Ethical considerations are generally of high importance and by using methods of preclinical imaging (here DLIT/µCT), animals can be examined longitudinally and serve as their own control if involved in therapy studies. This significantly reduces the number of animals required in a study to obtain meaningful data [49] which contributes effectively to the realization of the 3R concept and means reduction, refinement and replacement [50]. Here, the imaging procedures followed a strict protocol including cell injection, growth monitoring and final tumour removal. However, after excision of the primary tumour in all animals, except one individual, only residual cancer cells were detected, which were located at the site of injection in the skin. These residual cells grew to secondary lesions later on. Only one animal showed distant metastasis after resection of the primary tumour in inguinal and axillar lymphnodes. However, also in this animal residual cells from the primary tumour could be detected in the skin as well. Another animal showed distant metastasis, after a small secondary skin associated tumour was resected, but this signal disappeared and the animal was considered tumour free. Generally the CMT-U27 model can be considered as slow growing. This, and the fact that only the animal with the slowest growing tumour (animal number 90) showed distant metatastasis after removal of the primary tumour, leads to the hypothesis that cells need time to develop the ability to invade lymphatic vessels while local invasiveness is very well developed. Two animals furthermore showed distant metastasis after removal of secondary skin lesions, which supports the time hypothesis. A second option may be that despite injecting into the mammary fat pad, the infiltration of the skin is part of the metastatic process. The local invasiveness leads to further problems, as these residual tumours potentially grow to a size which requires euthanasia or repetitive surgery, which is not desirable when considering animal welfare. Although the study did not lead to the desired outcome to generate a reliable spontaneously metastasizing rodent model of canine breast cancer, longitudinal combined DLIT/µCT analysis qualified itself as a method to unmask changes in the tumour microenvironment by visualizing changes in spatial DLIT signal distribution within the tumour volume. The ability to precisely derive tumour volume from µCT images and to relate

the DLIT signal strength can be a quantitative measure for changes within the tumour microenvironment.

DLIT signal does not reflect tumour load especially when tumours grow and exceed a certain size [51, 52, 53]. Beside the presence of luciferase positive cancer cells light emission can only take place if sufficient amount of luciferin, ATP and oxygen are available.

Hypoxic areas, caused by absence or insufficiency of vessels and/or areas of necrosis, cannot exhibit light emission. The presence of these factors proved to be prognostic markers for therapy response [54, 55]. While DLIT/µCT can indicate changes it cannot identify the individual underlying mechanisms due to limited soft tissue contrast of µCT. The fact that at later timepoint DLIT signal was mainly found at the tumour rim indicates a necrotic core, which could be proven by subsequent histologic examination.

For future studies, due to excellent soft tissue contrast, combined DLIT/MRI could be an even more precise method for providing the needed morphologic information as it can identify necrotic tissue and by applying contrast agents vascularisation can be derived. Furthermore the implantation of the CMT-U27 cells in scid mice could be tested and compared to the present nude model considering the different states of immunodeficiency and its effects on the metastatic behaviour. A further asset is that primary tumours grew in their natural environment (mammary tissue) as validated by histologic examination (Fig.1) and therefore exert all advantages related to orthotopic implantation, such as the better efficacy of metastatic processes [56], local invasion like angiogenesis [57] and the better effectiveness of chemotherapy in vivo [58, 59].

A further valuable aspect which qualifies the model as interesting for future therapy studies is that tumours grew to a relatively large size, comparable to the absolute size of a typical nodule without hampering animal welfare. In clinical tumour therapy even the distribution of active substances within the tumour volume is crucial to obtain anti cancer activity. This is often hampered by tumour volume and associated microenvironment such as leaky vascular structures, insufficient lymphatic drainage and resulting increased interstitial pressure [60]. The relatively large size of the nodules therefore effectively mirrors clinical situation in dogs and humans. With the ability to detect and quantify changes, this model and the associated imaging technique can be a valuable tool in evaluating the effects of various therapy approaches especially approaches aiming at normalizing tumour microenvironment with respect to vascularization.

6. References

[1] Weigelt B., Peterse J.L., van't Veer L.J. (2005) Breast cancer metastasis: markers and models. Nat Rev Cancer 5(8): 591-602

[2] Sleeckx N., et al. (2011) Canine mammary tumours, an overview. Reprod Domest Anim 46 (6): 1112-31

[3] Nik-Zainal S., et al. (2012) The life history of 21 breast cancers. Cell 149(5): 994-1007

[4] Wu M., et al. (2014) The effect of interstitial pressure on therapeutic agent transport: coupling with the tumor blood and lymphatic vascular systems. J Theor Biol 355: 194-207

[5] Moghimi S.M., et al. (2005) Nanomedicine: current status and future prospects. FASEB J 19(3): 311-30

[6] Turtoi A., et al. (2015) Intratumoral heterogeneity and consequences for targeted therapies. Bull Cancer 102:17-23

[7] Devaud C., et al. (2014) Tissues in different anatomical sites can sculpt and vary the tumor microenvironment to affect responses to therapy. Mol Ther. 22:18-27

[8] Paolini M., Khanna C. (2008) Translation of new cancer treatments from pet dogs to humans. Nat Rev Cancer 8:147-56

[9] Schiffman J.D., Breen M. (2015) Comparative oncology: what dogs and other species can teach us about humans with cancer. Phil Trans R Soc B 370: 20140231

[10] Chen Z.Y., et al. (2014) Advance of molecular imaging technology and targeted imaging agent in imaging and therapy. Biomed Res Int 2014: 819324

[11] Chatziioannou A.F. (2002) Molecular imaging of small animals with dedicated PET tomographs. Eur J Nucl Med Mol Imaging 29(1): 98-114

[12] Rabinovich B.A., Ye Y., Etto T., et al. (2008) Visualizing fewer than 10 mouse T cells with an enhanced firefly luciferase in immunocompetent mouse models of cancer. Proc Natl Acad Sci U S A 105(38): 14342–14346.

[13] Hounsfield G.N. (1973) Computerized transverse axial scanning (tomography). Br J Radiol 46: 1016-1022

[14] Kujoory M.A., Hillman B.J., Barrett H.H. (1980) High-resolution computed tomography of the normal rat nephrogram. Invest Radiol 15: 148–154

[15] Sato T., Ikeda O. (1981) X-ray tomography for microstructural objects. Appl Opt 20: 3880–3883

[16] Bartling S.H., Stiller W., Semmler W., Kiessling F. (2007) Small Animal Computed Tomography Imaging. Curr Med Imaging Rev 3: 45–59

[17] Badea C.T., Drangova M., Holdsworth D.W., Johnson G.A. (2008) In vivo small-animal imaging using micro-CT and digital subtraction angiography. Phys Med Biol 53: R319–R350

[18] Rudin M. (2013) Molecular Imaging: Basic Principle and Application in Biomedical Research.

[19] Schambach S.J., et al. (2010) Application of micro-CT in small animal imaging. Methods 50(1): 2-13

[20] Zagorchev et al. (2010) Micro computed tomography for vascular exploration. J Angiogenes Res 2:7

[21] Lalwani K., et al. (2013) Contrast agents for quantitative microCT of lung tumors in mice. Comp Med 63(6): 482-90

[22] Boll H., et al. (2011) Micro-CT based experimental liver imaging using a nanoparticulate contrast agent: a longitudinal study in mice. PLoS One 6(9):e25692

[23] Paulus M.J., et al. (2000) High Resolution X-ray Computed Tomography: An Emerging Tool for Small Animal Cancer Research. Neoplasia 2: 62–70

[24] Harvey E.N. (1916) The mechanism of light production in animals. Science 44: 208-209

[25] Harvey E.N. (1917) The chemistry of light production in luminous organisms. Publ Carneg Instn 251: 171-234

[26] McElroy W.D. (1947) The energy source for bioluminescence in an isolated system. Proc Natl Acad Sci USA 33: 342-345

[27] McElroy W.D. and Strehler B.L. (1949) Factors influencing the response of the bioluminescent reaction to adenosine triphosphate. Arch Biochem 22: 420-433

[28] Green A.A. and McElroy W.D. (1956) Crystalline firefly luciferase. Biochem Biophys Acta 20: 170-176

[29] White E.H., et al. (1961) The structure and synthesis of firefly luciferin. J AM Chem Soc 83: 2402-2403

[30] White E.H., et al. (1963) The structure and synthesis of firefly luciferin. J AM Chem Soc 85: 337-343

[31] Lembert N. (1996) Firefly luciferase can use L-luciferin to produce light. Biochem J 317: 273-277

[32] McElroy W.D. and DeLuca M. (1978) Chemistry of firefly luminescence. Bioluminescence in action: 109-127

[33] Branchini B.R., et al. (2001) The role of active side residue arginine 218 in firefly luciferase bioluminescence. Biochemistry 40: 2410-2418

[34] McElroy W.D. and DeLuca M. (1983) Firefly and bacterial luminescence: basic science and applications. J Appl Biochem 5: 197-209

[35] Bhaumik S., Ghambir S.S. (2002) Optical imaging of Renilla luciferase reporter gene expression in living mice. Proc Natl Acad Sci USA 99: 377-382

[36] Massoud T.F., Gambhir S.S. (2003) Molecular imaging in living subjects: seeing fundamental biological processes in a new light. Genes Dev 17(5): 545-80

[37] Loening M.A., et al. (2007) Redshifted Renilla reniformis luciferase for imaging in living subjects. Nat Methods 8: 641-643

[38] Sato A., et al. (2004) In vivo bioluminescence imaging. Comp med 54(6): 631-634

[39] Paroo Z., et al. (2004) Validating bioluminescence imaging as a high-throughput, quantitative modality for assessing tumor burden. Mol Imaging 3:117–124.10.1162

[40] Zabala M., et al. (2009) Evaluation of bioluminescent imaging for noninvasive monitoring of colorectal cancer progression in the liver and its response to immunogene therapy. Mol Cancer 8:2.10.1186/1476-4598-8-2

[41] Kuo C., et al. (2007) Three-dimensional reconstruction of in vivo bioluminescent sources based on multispectral imaging. J Biomed Opt 12(2): 024007

[42] Lim E., et al. (2011) Monitoring tumor metastases and osteolytic lesions with bioluminescence and micro CT imaging. J Vis Exp. (50): 2775.

[43] Egeblad M., Nakasone E.S., Werb Z. (2010) Tumors as organs: complex tissue that interface with the entire organism. Dev Cell 18(6): 884–901.

[44] Harris AL. (2002) Hypoxia – a key regulatory factor in tumour growth. Nat Rev Cancer 2(1):38-47.

[45] Hockel M and Vaupel P. (2001) Tumor Hypoxia: Definitions and Current Clinical, Biologic, and Molecular Aspects. J Natl Cancer Inst 93:266-276.

[46] Bredholt G., et al. (2015) Tumor necrosis is an important hallmark of aggressive endometrial cancer and associates with hypoxia, angiogenesis and inflammation responses. Oncotarget 6(37): 39676–39691.

[47] Krol M., Pawlowski KM., Skierski J., Rao NA., Hellmen E. (2009) Transcriptomic profile of two canine mammary cancer cell lines with different proliferative and anti-apoptotic potential. J Physiol Pharmacol 60 Suppl 1:95-106.

[48] Su B., Cengizeroglu A., Farkasova K., Viola JR., Anton M., Ellwart JW., Haase R., Wagner E., Ogris M. (2013) Systemic TNFα gene therapy synergizes with liposomal doxorubicine in treatment of metastatic cancer. Mol Ther 21(2):300-8.

[49] Cunha L., et al. (2014) Preclinical imaging: an essential ally in modern biosciences. Mol Diagn Ther 18(2):153-73.

[50] Chen PJ. (2017) Animal welfare officers in Australian higher education: 3R application, work contexts, and risk perception. Lab Anim 1:23677217705152.

[51] Keyaerts M., et al. (2008) Dynamic bioluminescence imaging for quantitative tumour burden assessment using IV or IP administration of D: -luciferin: effect on intensity, time kinetics and repeatability of photon emission. Eur J Nucl Med Mol Imaging 35(5):999-1007

[52] Moriyama EH., et al. (2008) The influence of hypoxia on bioluminescence in luciferase-transfected gliosarcoma tumor cells in vitro. Photochem Photobiol Sci 7(6):675-80.

[53] Saint-Hubert MD., et al. (2012) Bioluminescence imaging of therapy response does not correlate with FDG-PET response in a mouse model of Burkitt lymphoma. Am J Nucl Med Mol Imaging 2(3):353-61.

[54] Camps C., et al. (2008) hsa-miR-210 Is induced by hypoxia and is an independent prognostic factor in breast cancer. Clin Cancer Res 14(5):1340-8.

[55] Picci P., et al. (1997) Chemotherapy-induced tumor necrosis as a prognostic factor in localized Ewing's sarcoma of the extremities. J Clin Oncol 15(4):1553-9.

[56] Killion JJ., Radinsky R., Fidler IJ. (1999) Orthotopic models are necessary to predict therapy of transplantable tumors in mice. Cancer Met Rev 17, pp. 279-284

[57] Pasqualini R., Ruoslahti E. (1996) Organ targeting in vivo using phage display peptide libraries. Nature, 380, pp. 364-366

[58] Kuo TH., et al. (1993) Site-specific chemosensitivity of human small-cell lung carcinoma growing orthotopically compared to subcutaneously in SCID mice: the importance of orthotopic models to obtain relevant drug evaluation data. Anticancer Res, 13, pp. 627-630

[59] Fidler IJ., et al. (1994) Modulations of tumor cell response to chemotherapy by the organ environment. Cancer Metastasis Rev, 13, pp. 209-222

[60] Juntilla MR., de Sauvage FJ. (2013) Influence of tumour micro-environment heterogeneity on therapeutic response. Nature. 501(7467):346-54.